COMPENSATION FOR POLARIZATION MODE DISPERSION AND NONLINEAR BIREFRINGENCE IN A MULTICHANNEL OPTICAL FIBRE SYSTEM

DAVID WAFULA WASWA

Submitted in fulfilment of the requirements for the degree of

PHILOSOPHIAE DOCTOR

in the Faculty of Science at the
Nelson Mandela Metropolitan University

January 2009

Promoter: Prof A. W. R. Leitch

DEDICATION

To our Lord God, through Him all things were made.

ACKNOWLEDGEMENTS

My sincere gratitude goes to my promoter, Prof. Andrew W.R. Leitch for his vast guidance and support, making this work possible. I thank Dr. Timothy Gibbon for the several constructive discussions throughout the course of my research. I wish to thank Prof. Andrea Galtarossa and his research group members at Padova University, Italy, for allowing me to use their research facility for three months. I remain indebted to my fellow research group members for their truly invaluable collaboration, encouragement and advice. Special acknowledgement goes to Dr. Lorinda Wu and Gibeon Makiwa for proofreading this thesis. I gratefully acknowledge financial support from NMMU, Telkom (Pty) Ltd, the South African National Research Fund (NRF), the African Laser Centre (ALC) and the Technology and Human Resources for Industry Program (THRIP). Last but not least, my sincere gratitude goes to my wife, Naomi and my children Paul and Gideon. I am in no doubt of the endurance and loneliness caused by my being apart from them for the duration of this research.

CONTENTS

ABSTRACT

Polarization mode dispersion (PMD) is stochastic in nature and continues evolving in an unpredictable manner according to the changing environment. Nonlinear birefringence in multichannel systems alters the polarization states of the bits, so that they vary from one bit to the next in a way that is difficult to predict. These are the two major signal-impairment effects that are inherent in optical fibre transmission links which can seriously degrade network performance. It is therefore extremely challenging to compensate for both linear and nonlinear birefringence in multichannel systems.

The purpose of this thesis is to investigate the interaction between PMD and nonlinear induced birefringence in a fibre with consideration of mode coupling. A sound knowledge of this interaction is necessary in designing a linear and nonlinear polarization mode dispersion compensator for WDM systems, as was successfully carried out in this study.

The investigation shows that the effect of nonlinear birefringence alone depolarizes the signal, while in high PMD links where polarization mode coupling is high, the nonlinear birefringence effect couples with second-order PMD such that it may reduce the penalty and improve the signal DOP. Further investigation shows that when nonlinear birefringence becomes significant, asymmetry arises between the two principal axes of the fibre, such that it is only one axis which experiences the effect of nonlinear birefringence. It is found out that along this

axis, there exists a critical point in pump power where the nonlinear birefringence cancels PMD in the link and improves the signal.

An adaptive compensator to cancel PMD and nonlinear birefringence was designed based on feedforward DOP-monitoring signal. The compensator was tested both at laboratory level and on the Telkom buried fibre link and found to be functioning as intended. It was able to adaptively track and compensate PMD in the link in less than a second. The compensator was able to cancel PMD in the link up to a maximum of 30 ps. The compensator improved the DOP of the worst signal by more than 100%.

ABBREVIATIONS LIST

ASE amplified spontaneous emission

BER bit error ratio

DFB distributed feedback

DFE decision feedback equalizer

DGD differential group delay

DOF degree of freedom

DOP degree of polarization

DVV dispersion vector velocity

EDFA erbium doped fibre amplifier

FFE feedforward equalizer

FOPMD first-order effect of PMD

FPMD femtosecond polarization mode dispersion

FWM four wave mixing

GPSA general Poincaré sphere analysis

JME Jones matrix Eigenanalysis

LSB lower sideband

MZI Mach-Zehnder interferometers

NRZ non-return to zero

RMS root mean square

RZ return to zero

SCM subcarrier multiplexing

SOP state of polarization

SPM self-phase modulation

OA optical amplifier

OER optoelectronic regenerator

OFDM orthogonal frequency-division multiplexing

PC polarization controller

PCD polarization dependent chromatic dispersion

PD photodiode

PDL polarization dependent loss

PMF polarization maintaining fibre

PMD polarization mode dispersion

PSP principal state of polarization

PMDC polarization mode dispersion compensator

PSA Poincaré sphere analysis

USB upper sideband

WDM wavelength division multiplexing

XPM cross-phase modulation

CHAPTER 1

INTRODUCTION

The optical fibre transmission network has increased the need for signal processing. A laudable accomplishment has been to create networks that span continents or oceans to interconnect communication assets in major urban areas with no need to convert optical signals back and forth to electric form. This is happening at a time when society requires that we have access to information at our finger tips *when we need it, where we need it, and in whatever format we need it.* Thus the saying *"Technology brings the world to the people and takes the people to the world"*. This ever-growing demand for the high speed communication has forced networks to use higher bit rates and transmission powers.

In the optical telecommunications field, one of the most significant developments has been the introduction of the erbium-doped fibre amplifier (EDFA) in the late 1980s and early 1990s, which allows all-optical signal amplification to take place simultaneously on many wavelengths within the 1550 nm window. Over the time EDFA has become increasingly sophisticated with wider wavelength coverage and higher output powers. Thus, fibre losses are no longer a major limiting factor for optical communication systems.

Nonlinear effects have become significant at high optical power levels and have become more important since the development of EFDA and wavelength division multiplexed (WDM) systems. By increasing the capacity

of the optical transmission line, which can be achieved by increasing channel bit rate, decreasing channel spacing or the combination of both, the fibre nonlinearities come to play an even more decisive role.

The origin of the nonlinearities is the refractive index of the optical fibre, which is varying with the intensity of the optical signal. The high signal intensity associated with the large number of channels at closely spaced wavelengths may introduce problematic nonlinear effects such as four-wave mixing (FWM), self-phase modulation (SPM) and cross-phase modulation (XPM). Thus intensity-dependent refractive index is a major source of nonlinear birefringence whose effect is nonlinear polarization rotation. However, many strategies such polarization multiplexing and interleaving have been employed to reduce nonlinear effects in the transmission link. Using orthogonal polarization states of light, it is possible to add an extra set of channels to those split by wavelength in transmission systems based on WDM.

One of the remaining hurdles to high speed long-haul data transmission is the linear birefringence phenomenon of polarization mode dispersion (PMD). The statistical nature makes PMD difficult to measure and to compensate. Nevertheless, it is an impairment that can damage a transmission system, particularly when the bit rate is larger than 10 Gb/s or the fibre has poor PMD performance.

PMD compensation in a multichannel system is extremely challenging given that the behaviour of the state of polarization (SOP) in each channel is

different in the optical domain. Generally, PMD compensation must be adaptive in order to track and cancel the fast PMD in the link. The challenges come when the interaction of PMD and nonlinear effects causes the SOPs to rotate faster than the speed with which the compensator could track them, and thus destroys the compensation. It is important therefore to analyze the interaction between PMD and nonlinear effects in the transmission system and come up with better ways of overcoming the combined effects.

This thesis is arranged as follows. Chapter 2 contains an overview of linear effects in optical fibre, followed by chapter 3 which introduces the techniques and methods of compensation or mitigation for polarization mode dispersion. Chapter 4 covers the review of nonlinear effects in optical fibre. In this chapter, causes and effects of nonlinearities on the polarization state in WDM channels, the nonlinear polarization evolution in birefringent fibres, and the interaction of linear and nonlinear polarization rotation, are reviewed. Chapter 5 consists of simulation and experimental results of the analysis of interaction between PMD and nonlinear birefringence in a WDM system. Chapter 6 starts with results of characterization the first-order PMD compensator followed by the design, control and results of experimental test of the PMD multichannel compensator. Lastly, chapter 7 brings out the summary of the important findings of the thesis.

CHAPTER 2

LINEAR EFFECTS IN OPTICAL FIBRE

In this chapter we briefly go through the theory of lightwave polarization, which provides the background for the study of depolarization in single-mode fibre. Polarization plays an important role in the interaction of light with matter.

2.1 Concept of Polarized light

Polarization is a property of electromagnetic radiation describing the shape and the orientation of the electric field vector as a function of time, at a given point in space.

If light is assumed to propagate in the positive z-direction, the real instantaneous electric field vector can be written as a superposition of two orthogonal components in time t [1] as

$$\mathbf{E}(z,t) = \mathbf{i}E_{0x}e^{i(\beta_x(\omega)z - \omega t + \varphi_x)} + \mathbf{j}E_{0y}e^{i(\beta_y(\omega)z - \omega t + \varphi_y)} \qquad (2.1)$$

where $\beta_{x,y}(\omega) = \frac{\omega}{c} n_{x,y}(\omega)$, E_{ox} and E_{oy} are the maximum amplitudes in the x- and y-axis, φ_x and φ_y are the corresponding phases respectively, ω is the angular frequency, c is the speed of light and n is the refractive index of the

waveguide. The equation of the locus of **E** is obtained by eliminating t in Eq (2.1) and assuming that z= 0, setting $\phi = \phi_x - \phi_y$, thus

$$\left(\frac{E_x}{E_{ox}}\right)^2 + \left(\frac{E_y}{E_{oy}}\right)^2 + 2\frac{E_x E_y}{E_{ox} + E_{oy}}\cos(\varphi) = \sin^2(\varphi) \qquad (2.2)$$

This equation is a representation of elliptically polarized light and the trace of the state of polarization (SOP) is as shown in Fig. 2.1. The angle α is the SOP orientation angle relative to the x-axis.

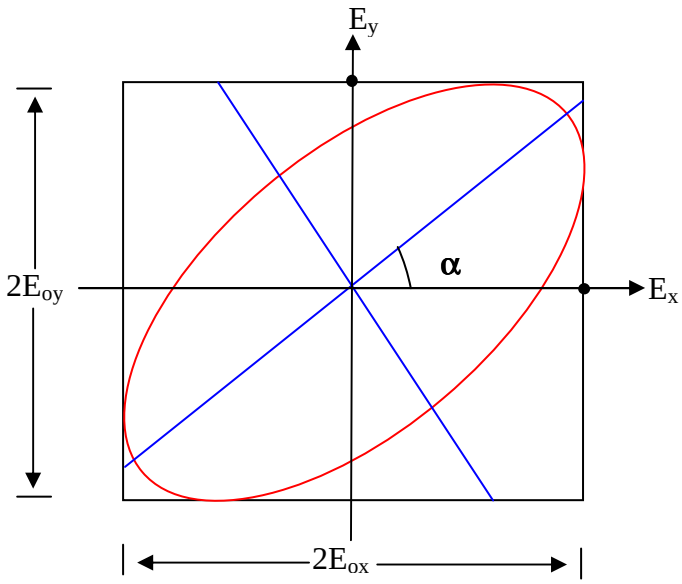

Fig. 2.1: Elliptically polarized light oriented at an angle relative to the x-axis having components of amplitude $2E_{oy}$ and $2E_{ox}$.

When the phase $\phi = \pm n\pi$ (n = 0, 1, 2 …) the ellipse collapses into a straight line and it corresponds to a linearly polarized light with a constant orientation and varying amplitude. When $\phi = \pm(2n+1)\,\pi/2$, (n = 0, 1, 2 …) there is constant amplitude (E_{ox} = E_{oy}) but varying orientation giving circularly

polarized light. Elliptically polarized light has both varying orientation and amplitude.

2.2 Jones and Stokes formalism

Polarized light can be represented by a two-element complex vector; the elements specify the magnitude and phase of the x- and y- components at any particular point in time. The following equation represents the Jones vector [2]:

$$\mathbf{E} = \begin{pmatrix} E_x \\ E_y \end{pmatrix} = \begin{pmatrix} E_{0x} e^{i\varphi_x} \\ E_{0y} e^{i\varphi_y} \end{pmatrix} \tag{2.3}$$

The Jones vector describes the polarized radiation components of the *E-M* wave. However, in the general case, the propagating wave may consist of a polarized component and not polarized component. Therefore, the propagating lightwave is well described by the Stokes vector $\boldsymbol{S} = [S_0, S_1, S_2, S_3]$ in which each of the four parameters is defined in terms of the two components ellipticity, χ and the orientation, ψ as

$$S_0 = \frac{E^2}{E_0^2} \tag{2.4}$$

$$S_1 = \cos 2\chi \cos 2\psi \tag{2.5}$$

$$S_2 = \cos 2\chi \sin 2\psi \tag{2.6}$$

$$S_3 = \sin 2\chi \tag{2.7}$$

The three normalized Stokes vectors s_1, s_2, and s_3 are coordinates on the Poincaré sphere that define the unique state of polarization described by ellipticity, χ and the orientation,ψ as shown in Fig.2.2.

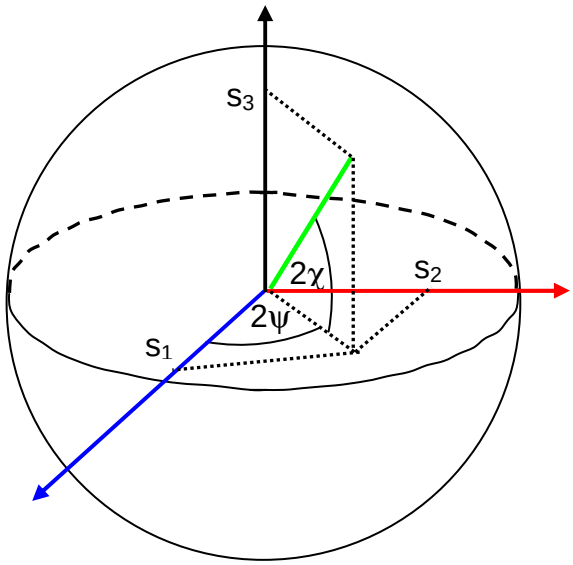

Fig. 2.2: Representation of Stokes parameters on the Poincaré sphere.

On the Poincaré sphere, the poles (where $\chi = 45^o$) correspond to the circular polarization and the equator (where $\chi = 0^o$) represents all linear polarizations. The total intensity (polarized and unpolarized light), $I_{tot} = S_0$, while the intensity for polarized light, $I_{pol} = \sqrt{S_1 + S_2 + S_3}$. The ratio of intensity of the polarized light to the total intensity is called the degree of polarization (DOP) [3], given as

$$DOP = \frac{I_{pol}}{I_{tot}} = \frac{\sqrt{S_1 + S_2 + S_3}}{S_0}, 0 \le DOP \le 1 \qquad (2.8)$$

If DOP = 0, the light signal is not polarized and its Stokes vector will be found within the volume of the Poincaré sphere while if DOP = 1, the light signal is

completely polarized and the Stokes vector will be located on the surface of the unit sphere.

2.3 Linear effects

There are two linear dispersions in an optical fibre namely, chromatic dispersion and polarization mode dispersion (PMD). Chromatic dispersion does not form a part of this research hence it will not be discussion further in this thesis.

2.3.1 Polarization Mode Dispersion (PMD)

Single-mode optical fibres ideally are supposed to maintain a single polarization state even after long distance transmission. In practice, the optical pulse propagates along single-mode fibre in two polarization modes [4] due to asymmetry in the fibre cross-section. The consequence of this asymmetry of cross-section is the existence of optical birefringence. As a result, when light is transmitted through the fibre core, its vector is decomposed into two orthogonally polarized components having different group velocities. The pulses arrive at the output differentially delayed. This difference between the delays is termed as the differential group delay (DGD). The DGD is the measure of an effect known as polarization mode dispersion (PMD), which is a phenomenon that leads to pulse broadening and system impairments limiting the transmission capacity of the fibre [5-6].

2.3.2 Causes of birefringence and mode coupling

As we have mentioned earlier PMD has its origin in optical birefringence and the causes of this birefringence are the intrinsic and extrinsic perturbations in optical fibre. Intrinsic perturbations include the manufacturing process which causes permanent birefringence, while extrinsic perturbations include stress (which causes non circularity of the fibre core) and environmental changes like temperature and pressure. These factors and the pulse broadening effect are illustrated in Fig. 2.3. The perturbations change as the fibre's external environment changes [7-8].

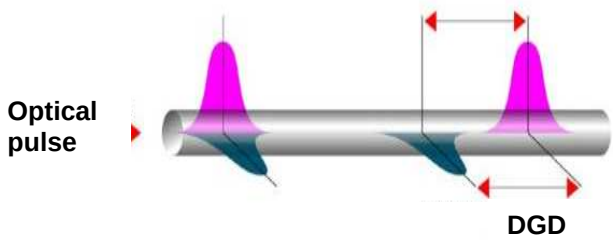

(a)

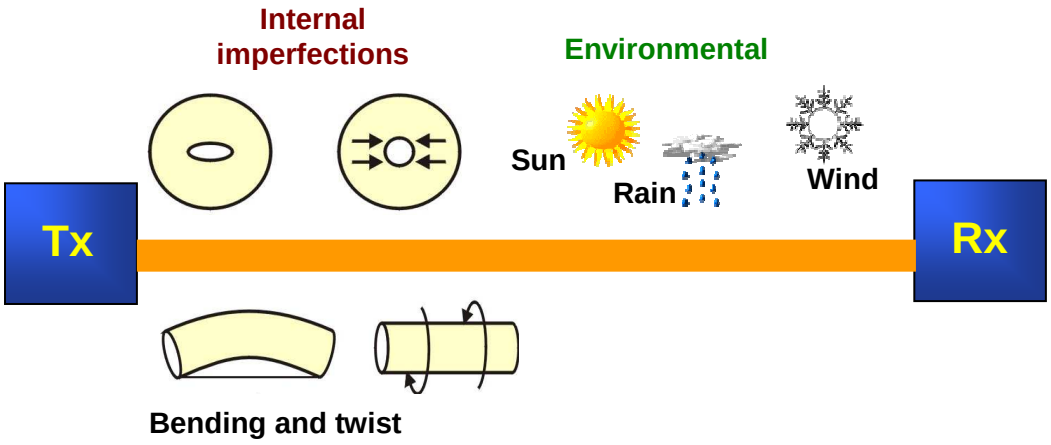

(b)

Fig. 2.3: (a) Effect of PMD in a birefringent fibre on optical pulse (b) Factors responsible for birefringence in optical fibre.

The birefringence difference between the fast and slow modes can be expressed as [9]:

$$\Delta\beta = \frac{\omega n_s}{c} - \frac{\omega n_f}{c} = \frac{\omega \Delta n}{c} \qquad (2.9)$$

where ω is the angular optical frequency, c is the speed of light and

$\Delta n = n_s - n_f$ is the differential refractive index between the slow and fast modes.

The length of birefringent fibre over which a complete revolution of polarization takes place is defined as the *beat length* (see Fig. 2.4), alternatively defined as the polarization distance for which the polarization state rotates through one cycle. The beat length is given by

$$L_b = \frac{\lambda}{\Delta n} = \frac{2\pi}{\Delta\beta} \qquad (2.10)$$

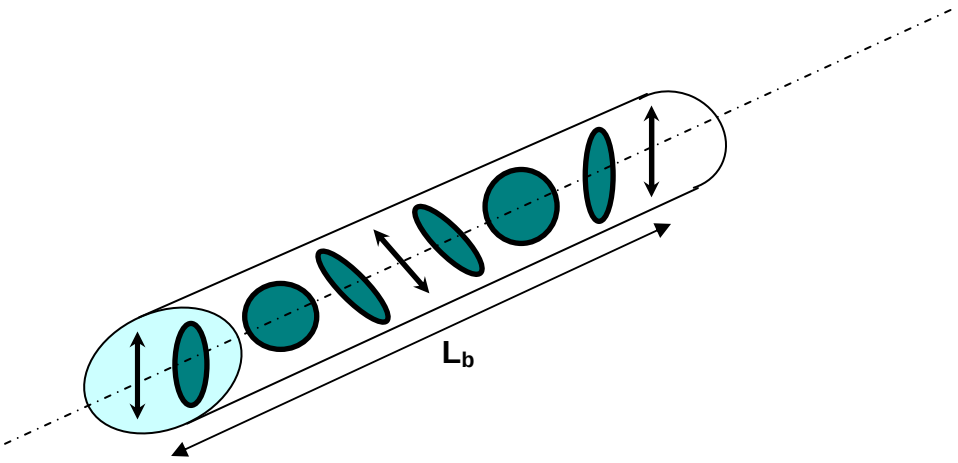

Fig. 2.4: Schematic illustration of polarization evolution and beat length

Polarization mode coupling

In long fibres with various kinds of extrinsic and intrinsic perturbations as mentioned above, there are random variations in the axes of the birefringence along the fibre length, causing random coupling of the two modes, known as polarization mode coupling. Mode coupling can also develop in long transmission systems, where the fibre link is composed of a large number of segments of single mode fibres having random lengths and random fusion angles between them. Each of these segments has its own slow and fast modes and a portion of the signal propagates on each of them. At the boundary between the sections, the polarization vectors will be resolved into new pairs of local modes belonging to the next segment. The process of rotating the polarization vector into the new modes of the following segment is also known as mode coupling. Mode coupling becomes an issue for lengths longer than 100 m [10]. In general, PMD is caused by the birefringence in the fibre and is complicated by mode coupling in the fibre link.

The mode coupling process allows the DGD to increase proportionally to the square root of the length of the fibre link [11]. Similarly, the *polarization mode dispersion coefficient* is defined as the PMD divided by the square root of fibre length (measured in ps/√km). The DGD does not increase linearly with highly mode-coupled fibres because occasionally, the coupling between segments reduces the accumulated DGD i.e. when the slow mode of one segment is aligned with the fast mode of the next or previous segment, the DGD of both segments will cancel out. It is the mode coupling phenomenon which makes the DGD and the fast and slow modes of the fibre to be frequency dependent

[12]. The statistical properties of PMD shows that the evolution of DGD at a particular frequency over time yields a Maxwellian probability function given by [13]

$$\mathrm{PDF}(\Delta\tau) = 3\sqrt{\frac{6}{\pi}}\,\frac{\Delta\tau^2}{\Delta\tau_{\mathrm{rms}}^3}\exp\left(-\frac{3\Delta\tau^2}{2\Delta\tau_{\mathrm{rms}}^2}\right) \qquad (2.11)$$

where $\Delta\tau_{\mathrm{rms}} = \langle\Delta\tau^2\rangle^{1/2}$.

In the absence of polarization dependent losses, the input (output) states of polarization launched into the two propagation modes are mutually orthogonal because there is nothing to break the degeneracy in the two supported modes. These states of polarization are commonly referred to as *principal states of polarization* (PSPs) [14]. In a graphical representation of polarization states, PSPs are located in diametrically opposite points on the Poincaré sphere's surface. The DGD measured as a differential transmission time, $\Delta\tau$, at any given wavelength of two undistorted signals polarized along orthogonal states of polarization constitutes what is known as *first-order effect* of PMD (FOPMD).

In other words, the PSP is defined as that input polarization for which the output state of polarization is independent of frequency to first order, i.e., over a small frequency range (bandwidth). It implies that any change of frequency within this bandwidth will not change the output polarization. Therefore DGD is frequency dependent while the PSP is frequency independent if only first-order PMD effect is being considered.

2.3.3 PMD vector

Based on the observation made in section 2.3.2, the PMD vector $\vec{\Omega}$, is defined as follows [15]:

$$\vec{\Omega} = \tau \vec{q} \qquad (2.12)$$

where τ is the magnitude of the PMD vector and is called the DGD, while $\vec{q}$ is the unit vector pointing in the direction of the slow principal state of polarization. Note that this definition does not follow that adopted by Poole [16].

For a polarization-maintaining fibre (PMF) with constant birefringence, the two eigenmodes coincide with the two principal axes of birefringence of the fibre. Optical pulses polarized along these two eigenmodes have either a maximum or minimum group delay. Unlike the PMF fibre, the birefringence of real fibre changes randomly along the fibre length in both magnitude and orientation [17]. According to Poole and Wagner [14] for narrow-band pulses, there exists a set of two orthogonal input states of polarization for which the corresponding output states of polarization are independent of frequency to first order. In general, an input signal initially aligned with a principal state will evolve through varying states of polarization as it propagates, in contrast to an eigenmodes in a PMF which propagates unchanged. The relationship between the principal states of polarization and DGD in a single-mode fibre was statistically determined [18]. The authors found that the DGD increases as the square root of the length when the length of the fibre is longer than the correlation length of the perturbations. Later, Shieh [19] proved that principal

states of polarization exist in random birefringent fibres having random mode coupling regardless of the spectral components of the optical pulses. These PSPs are effects of the birefringence and mode coupling over the entire fibre length, and may not necessarily be correlated with the local fibre birefringence.

2.3.4 Second-Order PMD

In a fibre having random birefringence, beyond the first order PSPs bandwidth, it is known that PSPs are frequency sensitive [14, 20]. It therefore means that each frequency sees a different pair of polarization modes and undergoes different time delays. Hence DGD becomes frequency dependent. In addition, the relative power launched into each of the two polarization modes may also vary in time, thus the output signal is distorted. This phenomenon is called *second-order PMD* (SOPMD).

Following the above argument, SOPMD effects are due to frequency dependence of the DGD and PSPs [21]. The frequency derivative of equation (2.12) then provides the mathematical definition of SOPMD as follows:

$$\vec{\Omega}_{\omega} = \frac{d\vec{\Omega}}{d\omega} = \frac{d\tau}{d\omega}\vec{q} + \tau\frac{d\vec{q}}{d\omega} = \tau_{\omega}\vec{q} + \tau\,\vec{\mathrm{q}}_{\omega} \tag{2.13}$$

where subscript ω indicates differentiation with respect to frequency. The first term on the right $\tau_{\omega}\vec{q}$ represents the polarization-dependent chromatic dispersion (PCD), while the second term $\tau\,\vec{\mathrm{q}}_{\omega}$ represents the depolarization. The SOPMD vector and its components are shown in Fig. 2.5.

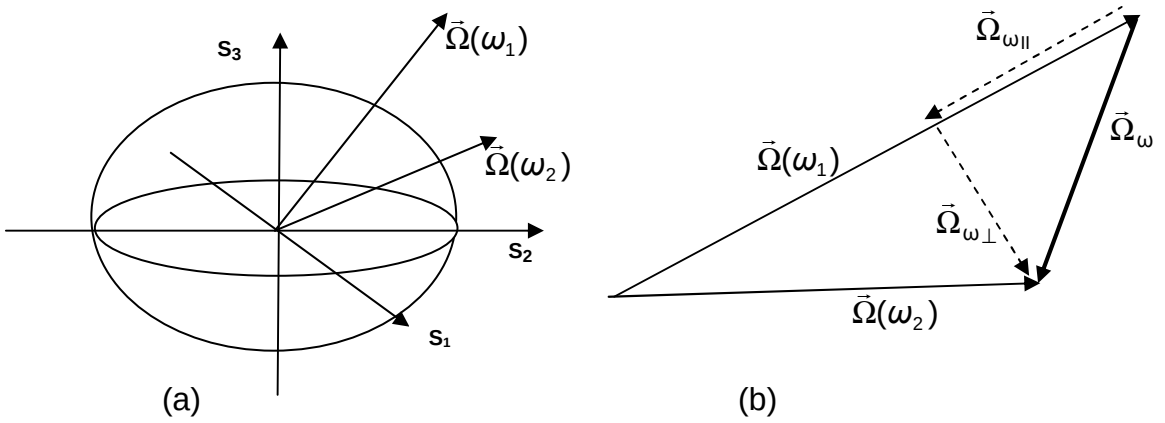

Fig. 2.5: Definition of SOPMD vector $\vec{\Omega}_{\omega}$. (a) Poincaré sphere diagram showing the PMD vectors $\vec{\Omega}(\omega_1)$ and $\vec{\Omega}(\omega_2)$. (b) SOPMD vector and its components. [22].

The depolarization component $\vec{\Omega}_{\omega\perp} = \tau \vec{q}_{\omega}$, runs perpendicular to $\vec{\Omega}(\omega_1)$ and indicates the rotation of the PSPs with frequency. The PCD component $\vec{\Omega}_{\omega\parallel} = \tau_{\omega} \vec{q}$, runs parallel to $\vec{\Omega}(\omega_1)$ and indicates the change of DGD with frequency. Theoretical and experimental results have shown that the depolarization component is dominant over the PCD component [23]. This is also demonstrated in our field measurement results in section 2.5.

Both the DGD and the depolarization correlate in such a way that the depolarization rate, $\vec{q}_{\omega}$ is large at wavelengths where the DGD is small and *vice versa* [24]. The impact of second-order PMD on the pulsewidth of the signal at the output of the fibre has been studied both in frequency and time domain [25-27]. It has generally been concluded that whenever average DGD is less than one tenth of the bit period, second-order PMD effect can be neglected.

2.4 The PMD measurement techniques

There are three principal PMD features that are of interest to measure, depending on application. One feature is the mean DGD [28]; it is the scaling parameter necessary to specify the statistics of all orders of PMD. Another feature is the PMD vector as a function of frequency [29]. This vector information is necessary to characterize the first- and higher-order PMD of a component or a fibre directly. The third feature is the direct measurement of the fibre birefringence as a function of position [30-32]. This technique has advantage over others. It allows not only measuring precisely the PMD but it also gives the complete view on the distribution of the total birefringence along the fibre.

2.4.1 Jones Matrix Eigenanalysis (JME) Technique

The Jones matrix method uses a set of predetermined launch polarization states to determine the complex Jones Matrix, **T**(ω), of the fibre at each frequency. An illustration of the JME technique is shown schematically in Fig. 2.6. Basically, a tuneable laser source is used as the input signal; this is swept through a range of wavelengths at the input of the fibre under test, the polarization controller generates three linear polarization states at each wavelength and the Polarimeter processes the measured results.

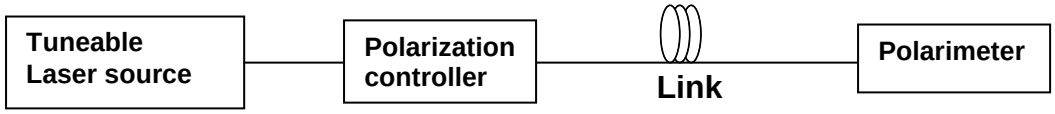

Fig. 2.6: Setup of JME method used for measuring PMD

From the Stokes parameters, the response Jones matrix at each wavelength is computed. For each wavelength interval, the product of the Jones matrix $\mathbf{T}(\omega + \Delta\omega)$ at the higher optical frequency and the inverse Jones matrix $\mathbf{T}^{-1}(\omega)$ at the lower optical frequency are computed. The eigenvalues of successive matrix products $\mathbf{T}(\omega+\Delta\omega)\mathbf{T}^{-1}(\omega)$ are determined. One can then compute the frequency derivative and from this the differential group delay at frequencies $\{(\omega+\Delta\omega) + (\omega)\}/2$ is determined using [29]

$$\Delta\tau = \left| \frac{Arg\left(\frac{\rho_1}{\rho_2}\right)}{\Delta\omega} \right| \qquad (2.14)$$

where *Arg* represents the argument function, that is, $\mathrm{Arg}(\eta e^{i\theta}) = \theta$ and, ρ_1 and ρ_2 are the eigenvalues of $T(\omega+\Delta\omega)T^{-1}(\omega)$.

At the end of the measurement, several values of DGD are obtained, from which the mean DGD is then calculated. The second-order components, PCD and depolarization can also be determined from the angular frequency derivative of the PMD vector as outlined in section 2.3.4. This has been the main technique applied in this work to determine the first- and second-order PMD as demonstrated in the results to be presented in section 2.6.

2.4.2 Poincaré Sphere Analysis (PSA) Technique

The experimental setup of PSA is the same as that one used in JME but the difference between the two techniques is in the methods of analyzing the data.

The PSA technique works with derivatives of the measured Stokes vectors rather than the polarization transfer matrix. For linear polarization launch states at approximately 0°, 45°, and 90°, the corre sponding output polarization states are measured at two closely spaced wavelengths. The three Stokes parameters ($\hat{h}, \hat{q}$ and $\hat{c}$) are measured at the output of a fibre as a function of frequency. For a link without PDL, the DGD can then be given as [33].

$$\partial\tau = \left|\vec{\Omega}\right| = \sqrt{\frac{1}{2}\left[\left(\frac{d\hat{h}}{d\omega}\right)^2 + \left(\frac{d\hat{q}}{d\omega}\right)^2 + \left(\frac{d\hat{c}}{d\omega}\right)^2\right]} \qquad (2.15)$$

We used this technique to measure second-order PMD at the laboratory. A FPMD-5600 Femtosecond PMD analyzer of EXFO in Canada [34] was used. The parameters that are measured by the instrument are: the second-order PMD vector (this is also known as the dispersion vector velocity (DVV)), the DGD, the PSPs and the Stokes vectors. The components of SOPMD are not measured directly but they can be determined using the following equations [34]:

$$DVV = \sqrt{(\text{parallel})^2 + (\text{perpendicular})^2} \qquad (2.16)$$

where “parallel” refers to the PCD, while “perpendicular” refers to the depolarization component. The PCD component is given by

$$PCD = 2\pi DVV \qquad (2.17)$$

The depolarization component then can be determined from PCD and DVV.

2.4.3 Advantages and disadvantages of JME and PSA techniques

Advantages of JME

The JME method allows one to simultaneously evaluate the DGD, PSP and PDL per wavelength in the link. It has high sensitivity and accuracy. It enables one to troubleshoot a link by measuring DGD at each wavelength.

Disadvantages

It is slow in processing results.

Advantages of PSA

The PSA technique allows a complete dispersion vector to be measured as function of wavelength, thus yielding information about the PSPs and higher order dispersion. It has high accuracy for both large and small values of PMD which is usually being limited by the stability of the device under test.

Disadvantages

The drawback of the PSA method is that it needs a fast Polarimeter, which is usually an expensive instrument.

2.5 Comparison of results obtained based on JME and PSA techniques

In this section the similarity and difference between two instruments that are used to measure first- and second-order PMD are demonstrated. The two instruments are; polarization analyzer (manufactured by Adaptive Photonics), and Femtosecond PMD (FPMD) analyzer of EXFO instruments, known as the FPMD-5600, based on the Generalized Poincaré Sphere Analysis (GPSA) [33]. The analysis was performed by measuring first- and second-order PMD of the emulators at the laboratory.

Fig 2.7 shows the measurement set-ups used. For the GPSA set-up, light from the ASE source passes through a hybrid Michelson interferometer and a SOP generator (polarization controller) before it is coupled into fibre link. In the JME method, light from a tuneable laser source passes through a polarization controller before it is coupled into the fibre link. The polarimeter at the end of the link is to measure the power and SOP of each wavelength. The link consists of a 24 km spool of standard single-mode fibre and PMD emulator made of PM fibre concatenated at random angles.

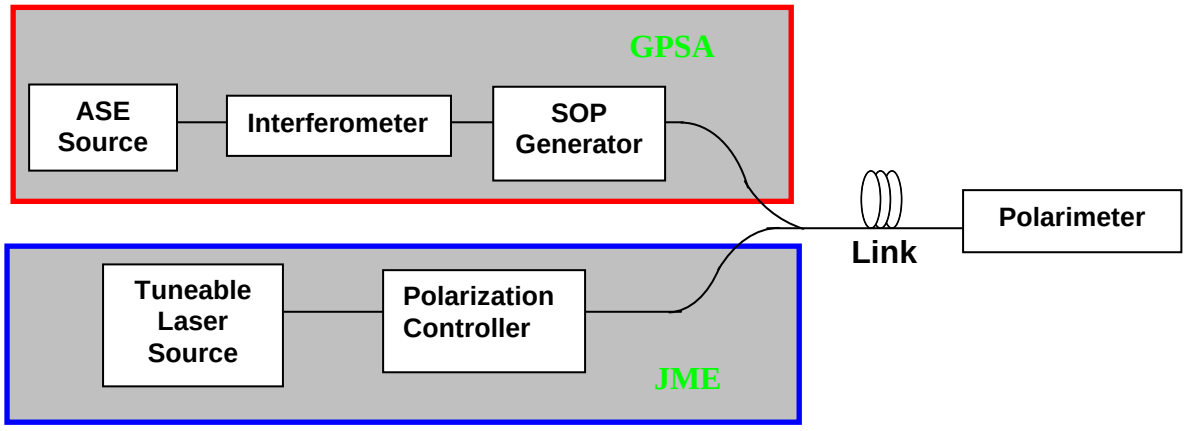

Fig. 2.7: Experimental setups used to measure second-order PMD based on JME and PSA methods.

The measurements were performed in the wavelength range of 1535 to 1565 nm with a wavelength step of 0.1 nm, yielding 1000 data points. The results obtained are shown in Fig. 2.8 to Fig. 2.10 below.

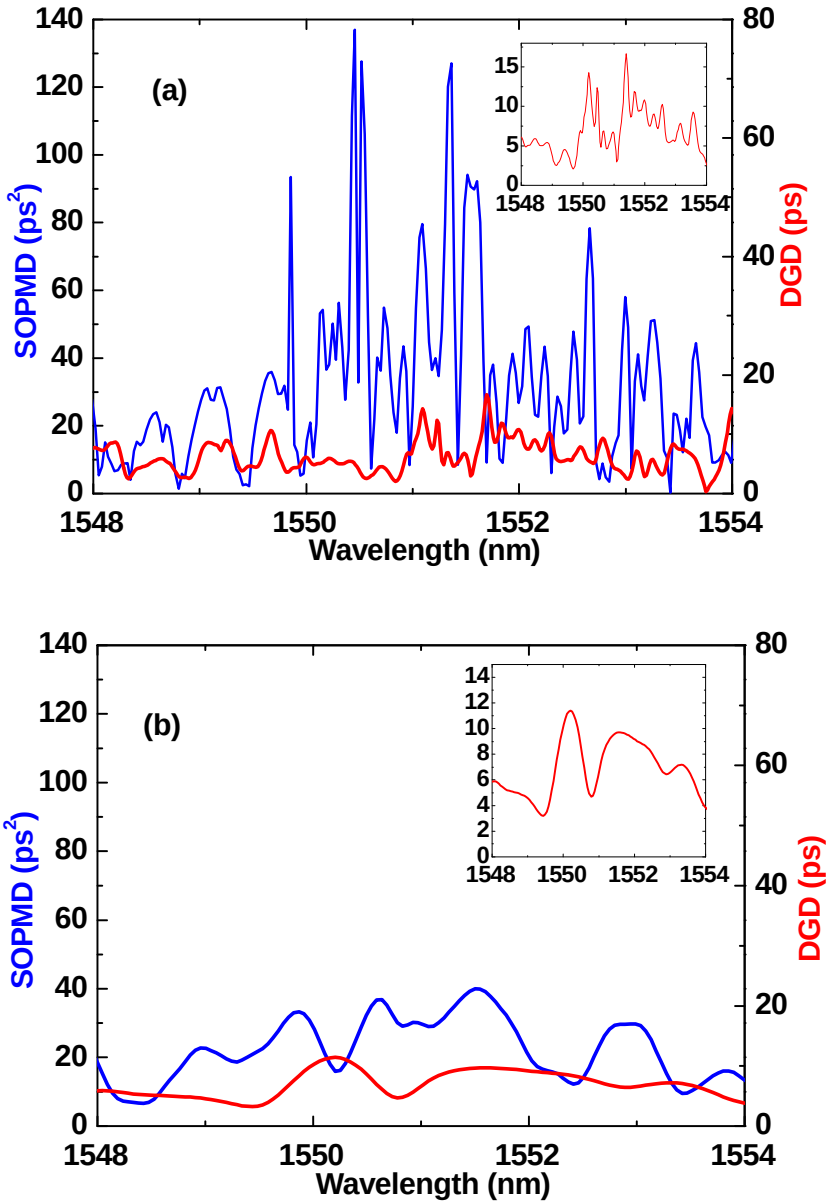

Fig. 2.8: Measurement of first- and second-order PMD using (a) Using GPSA (b) JME. The insets in (a) and (b) refer to the DGD data on magnified scales.

The average DGD values measured using the JME and GPSA methods were 6.6 ps and 6.9 ps, while the SOPMD values were 24 ps^2 and 47 ps^2 respectively. The DGD measurements using two techniques are identical,

while there is a noticeable difference in SOPMD measurements using the two techniques as seen in Fig. 2.8(a) and Fig. 2.8(b). The difference is due to the fact that the PSA method allows a complete characterization of PMD in a spectral range of arbitrary interval, thus yielding more information about the PSPs and higher order dispersion. Thus higher accuracy for both large and small values of PMD measurements is achieved.

The second-order PMD and its components were compared, as illustrated in Fig. 2.9. The eqs. 2.16 and 2.17 were used to calculate the components of second-order PMD; depolarization and polarization dependent chromatic dispersion (PCD). It is observed that the magnitude of depolarization is very close to the magnitude of SOPMD. Depolarization is therefore the dominant component in SOPMD [35].

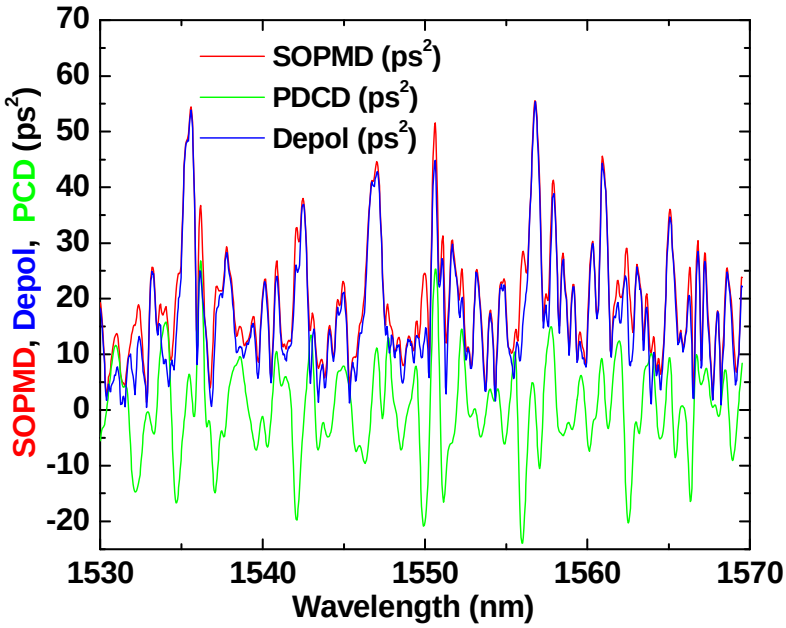

Fig. 2.9: Variation of second-order PMD, depolarization and polarization dependent chromatic dispersion with wavelength

As observed in Fig. 2.10(a) and (b), one can obtain unbiased results with a smaller error when using GPSA than using JME, this is because the mean value of the ratio of depolarization to SOPMD using GPSA is closer to the standard value than using the JME method. The standard value can be found in Refs [36-37].

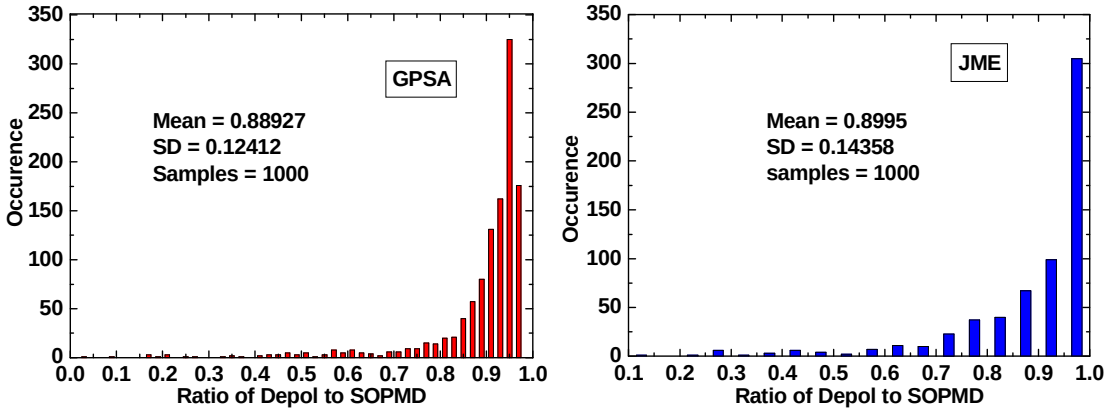

(a) (b)

Fig. 2.10: Occurrence of the ratio of depolarization to second-order PMD. (a) GPSA (b) JME

As a matter of caution, the GPSA based instrument is better for laboratory work than field work because it is slow in processing the data. Therefore for our field measurements we used the JME based instrument.

2.6 Field measurements of first- and second-order PMD

Before compensation was carried out it was necessary to measure the PMD on the fibre links. PMD tests were carried out on twenty deployed fibres, connected between two stations at Port Elizabeth, South Africa. The twenty fibres were in the same cable and pairs were looped to form a round trip distance of 28 km.

As was mentioned earlier, the JME technique was used to measure the DGD, SOPMD and its components (depolarization and PCD). The measurements were performed in the wavelength range of 1530 to 1570 nm with a wavelength step of 0.1 nm, yielding 1000 data points.

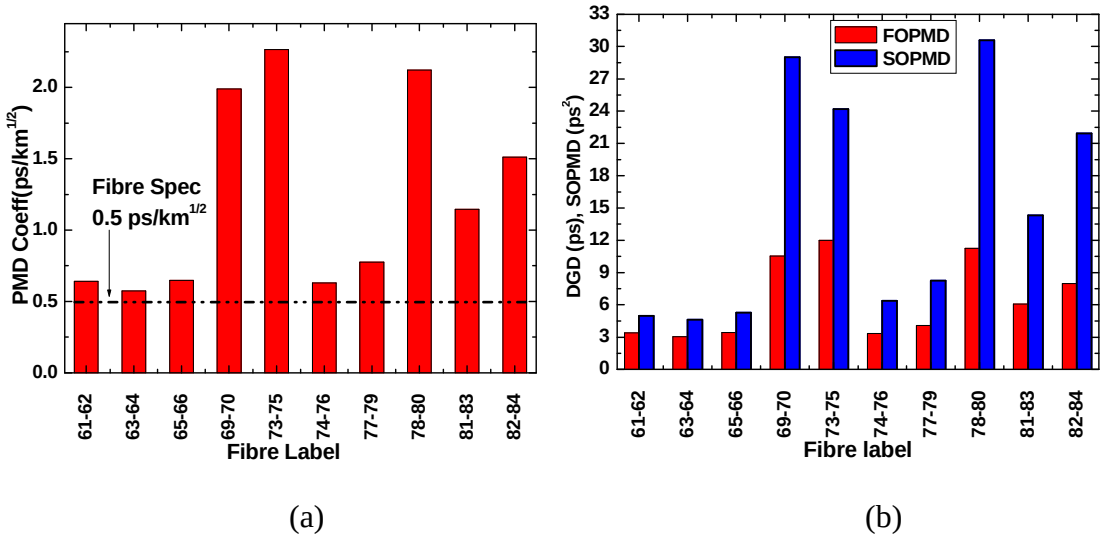

(a) (b)

Fig. 2.11: Field measurements of first- and second-order PMD. (a) The PMD coefficient in each link, with the dotted line indicating the threshold value for the deployed fibres. (b) The average of DGD and SOPMD in each looped link.

Fig. 2.11(a) shows the PMD coefficient in the test fibres used. The dotted line shows the maximum PMD coefficient permissible (0.5 ps/km$^{1/2}$) if the fibres have to carry the data at 10 Gb/s. None of the fibres is able to pass the test for PMD. This implies that either the old fibres need to be replaced or the mitigation/compensation systems are put in the links to counter the PMD in the link. Fig. 2.11(b) shows the average DGD and SOPMD in the link. For compensation studies (to be reported in Chapter 6) three fibres with the highest DGD were combined (69-70, 73-75, 78-80). This was to create the worst case scenario in the system to be compensated.

CHAPTER 3

POLARIZATION MODE DISPERSION COMPENSATION

In this chapter we shall consider the background to PMD compensation and review the two basic types of PMD compensators (PMDC). We then move on to a brief review of factors that determine the quality of a PMD compensator, as well as the optical PMD compensation monitoring techniques that are used. Lastly, we shall review the optical PMDC schemes where the compensator is classified according to its versatility and capability.

3.1 Background to PMD compensation

For many years efforts have been focused on strategies for reducing the effects of PMD in optical fibres as it has become evident that some commercial fibre optic cables may have PMD values unacceptable for certain network upgrade [38-40]. Ongoing strategies have also focused on reducing the intrinsic PMD of the fibre by altering the manufacturing process [41-43]; this has led to exceptionally low values of PMD in the new generation of single-mode fibre being manufactured.

Compensation for PMD effects is the alternative strategy that has led to significant increase in PMD tolerance [44-46]. Such strategies include the reduction of intersymbol interference (ISI) by electronic equalization in the

receiver [47-48] and optical equalization techniques that employ automatic polarization control at the receiver or transmitter [44-45, 49].

Electronic equalizers are applied after optoelectronic conversion of data signals. Both polarization modes carrying the noise are mixed on the photodiode. Thereafter PMD is assumed as ISI. The equalization is performed by using the linear and nonlinear adaptive electronic filters like the decision feedback equalizer (DFE) and the feedforward equalizer (FFE) [50-52]. The optimized filter transfer function is given by the matched filter characteristics to optimize the signal to noise ratio of the data signal [47]. In optical transmission, the electrical equalizers can only achieve limited performance due to nonlinearity of square law detection of the photodiode especially for advanced modulation formats causing loss of phase and polarization information [53-54].

On the other hand, the optical compensators are applied at the end of the fibre link output, before the receiver. The simplest compensator consists of a birefringent element in combination with a polarization controller (PC) that aligns the output SOP vector of the link to the axis of the birefringent element, so that the PMD vector can be cancelled. More detail in this regard will follow in the sections below. Successful compensation has been shown by adaptive electrical techniques at 10 Gb/s [55], and optical compensation in lab experiments and field trials performed at bit rates of 10, 40, and 160 Gb/s [56-57].

3.2 Factors determining the quality of an optical PMD compensator

The efficiency of a compensator depends on three factors: Firstly, *flexibility of the system*: The system should be adaptive in order to track the link output SOPs. Secondly, *the system should be fast*: Depending on the origin of PMD, fluctuations are observed in the time scale from days down to milliseconds [58-59]. The compensator should be able to change according to the time scale of SOP change. Thirdly, the number of *degrees of freedom* (DOF) should be small. The degree of freedom denotes the tuning parameters of the compensator which are necessary for adaptation. The number of DOF is most likely to determine the speed of the compensator. The higher the number of DOF, the lower will be the efficiency of the compensator. Suitable compensator adaptation schemes are necessary to meet speed and accuracy requirements of the system application. But we should also note that a compromise for PMD compensator complexity may lead to a limitation of its efficiency.

3.3 Optical PMD compensation monitoring techniques

An optical PMD compensator typically comprises of a polarization controlling device, an optical delay element (e.g. polarization maintaining fibres [44], [60], $LiNbO_3$ delayline [61] and Bragg gratings [62]) and an optical or electrical detector which provides control signals to the optical components based on information about the link's PMD.

Every PMD compensator that uses a feedback/feedforward control system requires some sort of distortion detection. The distortion detector monitors the

quality of the signal, and sends the information to the control algorithm; the control algorithm uses this information to adjust the parameters of the PMD compensator to match it to the current SOP of the signal or PMD vector of the link. A summary of the monitoring techniques used in feedback based, optical PMD compensation systems are given below.

3.3.1. Radio Frequency (RF) signal

This technique uses the power levels of specific tones in the received RF spectrum of the baseband signal [63]. Generally, PMD causes a reduction of power in the main lobe of the received baseband spectrum and therefore, the amount of PMD to be compensated for can be estimated by measuring the power level of a single tone that can give an unambiguous estimate of PMD. A drawback of using the above described technique is that the required hardware is bit-rate dependent. The photo-detector, band-pass filter, RF amplifiers etc can be used for one data rate only.

3.3.2 Degree of polarization (DOP) of the received optical signal

The DOP of a signal at the receiver end depends on the DGD of the system, the polarization splitting ratio and the signal pulse width. As the width of the pulse decreases, the DGD monitoring range provided by DOP monitoring decreases as well. The pulse splitting induced by PMD results in a time-varying state of polarization along the pulse, this therefore reduces the DOP (since DOP is a measure of the amount of optical power that is in the polarized state). The definition of DOP is based on the Stokes parameters (as

shown in section 2.2), and is routinely measured by a polarimeter-based instrument. A DOP ellipsoid has been used as a PMD monitor for compensation [64]. In this case, the transmitter provided polarization-scrambled pulses which passes through the fibre link and the polarimeter measured the pulse-averaged output SOPs of the signal. In this way the effect of PMD for input polarizations was sampled all over the Poincaré sphere. The nature of the ellipsoid is such that it provides information about both the PSPs and DGD of the link being monitored as indicated in Fig.3.1. The DOP of unity corresponds to the output of either the slow PSP or fast PSP. The DGD of the fibre is related to the minimum DOP of all the ellipsoid points.

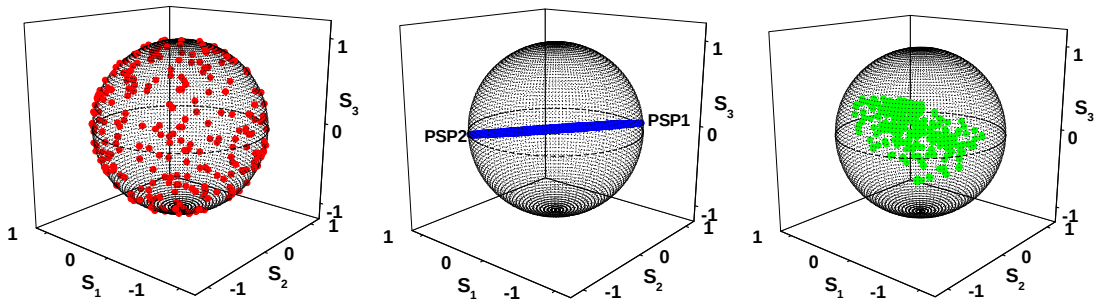

(a) (b) (c)

Fig.3.1: Ellipsoid for (a) Patch cord with negligible DGD (b) PM Fibre showing the PSPs (c) Emulator with DGD of 8 ps

The DOP as a monitoring parameter has also been used in multi-channel systems. Averaged-DOP monitoring of WDM channels for PMD compensation was demonstrated [65], where the DOP of each channel was measured and the DOP for all channels was averaged to yield a single monitoring signal for a single compensator. A DOP-based PMD monitor for subcarrier multiplexing (SCM) systems that has enhanced DOP sensitivity to DGD/PMD was

demonstrated [66]. The technique of optical filtering to improve the performance of DOP-based DGD monitoring was applied to equalize the optical power of the carrier and two sidebands. Using this method the DOP sensitivity to DGD was doubled. This is the technique that was applied in our experimental work.

Generally, the DOP has several advantages as a signal monitor; 1) it is data rate independent [65]; 2) it does not need high speed electronics; 3) it can be applied to both feedback and feedforward PMDCs; 4) it is simple (DOP evaluation reduces hardware complexity); and 5) it is unaffected by chromatic dispersion. Unfortunately, DOP measurements as a function of DGD suffer from the following disadvantages 1) there is a small DGD monitoring window when measuring a short pulse return-to-zero (RZ) signal; 2) there is lack of sensitivity when measuring a non-RZ (NRZ) signal.

3.3.3 Receiver eye diagram

The effect of polarization mode dispersion on a transmission system is to cause eye closure which reduces the optical signal-to-noise ratio and increases the likelihood of transmission errors. The purpose of the PMDC is to try and maintain the eye opening. PMD compensation therefore can also be controlled using an eye monitor as feedback signal. This technique is based on inter-symbol interference caused by PMD in the link. The received eye diagram is monitored and a control signal based on the amount of eye opening is generated. One of the earliest demonstrations of eye monitoring was by Buchali *et al* [67] who used a SiGe integrated chip consisting of two decision circuits as the eye monitor, which had a high correlation to the BER.

Ideally, the PMDC should optimize the BER but since the BER signal cannot be measured with high accuracy within a short period of time, it cannot be used directly as a quantitative representative of PMD. More recently, the performance of a one-stage PMD compensator with different feedback signals was studied [68]. It was found that the eye opening as a monitor has the strongest correlation with BER, while the DOP had the worst correlation with BER. However if an optical filtering technique could be used [44, 66], the correlation between DOP and BER could improve. The DGD also was found not strongly correlated to the BER.

3.4 PMD compensation schemes

In this thesis, we have classified the PMDC into three categories: first-order PMDC, second-order PMDC and multichannel PMDC. The PMDCs are reviewed according to these classes.

3.4.1 First-order PMDC

The effect of first-order PMD alone is to split the signal into two, delaying one part with respect to the other. This effect is minimised when the input polarization state is aligned with a PSP and maximised when the two PSPs are equally excited.

First-order PMDC may be divided into two classes, the fixed delay PMD compensation and the variable delay PMD compensation. Fixed delay PMDC was among the first PMD compensation techniques to be experimentally

demonstrated [44, 49]. The compensator was inserted at the receiver end of the transmission link as shown in Fig. 3.2.

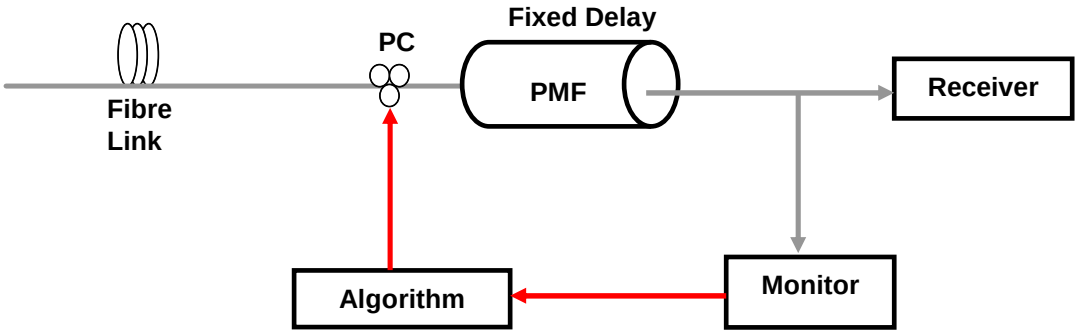

Fig. 3.2: Block diagram of fixed delay polarization mode dispersion compensator. Grey line indicates the fibre while the red line indicates electrical connection.

It consists of the PC and the polarization maintaining fibre or any fixed delay line. The PC aligns the output PSPs from the fibre link to the axis of PMF. In addition a feedback control signal was included to dynamically adjust the PC to achieve the best compensation performance. The concept used here is that the effect of PMD can be eliminated by confining the signal entirely to a single PSP.

Subsequently, Xie *et al* [69] showed analytically that there was an optimum delayline (polarization maintaining fibre) length for the PMD compensator and that this length decreased with increasing bandwidth. This implies that the larger the length of the birefringence fibre, the larger the induced SOPMD, which tends to degrade the overall PMD compensation performance. The fixed delay PMDC therefore can cause a risk of feedback loops trapping a locally-optimized state [61].

A more complex first-order PMDC was proposed to replace the fixed delay with variable delay, in order to detect and prevent being trapped in a non-optimum operation state and also to counter different amount of DGD values [45]. Fig. 3.3 shows the block diagram of such a first-order PMDC. The compensator comprised of a fast electro-optic polarization controller which connected the output of the transmission fibre to the input of a variable delay line. The output of the variable delay line was coupled to a motor-driven detector, which measured the PMD-induced distortion at the output of the compensator and generated a feedback control signal for the polarization controller and delay line. The control signals for the variable delay line and the polarization controller were based on the power level of the received base-band spectrum.

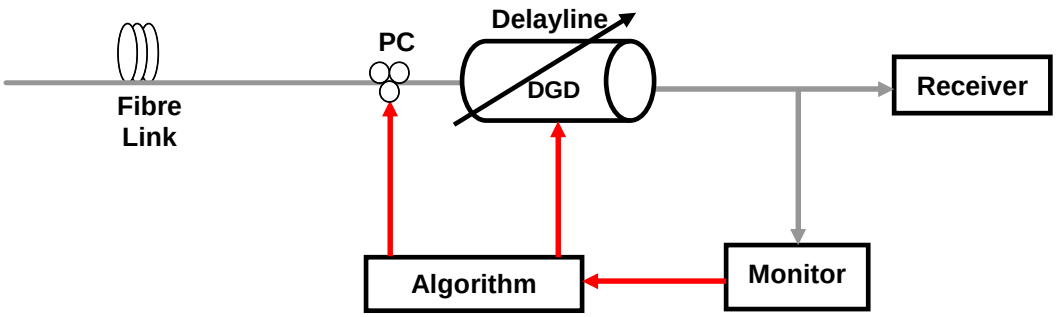

Fig. 3.3: Block diagram of first-order PMDC with variable delayline.

Using this design, Rosenfeldt *et al.* [70] demonstrated a 10 Gb/s PMDC using a polarization controller operated by a step motor and a variable delayline which was able to generate a maximum DGD of 140 ps. The BER was used as a control signal. A similar first-order compensator configuration was designed and tested in our Optical Fibre Laboratory. In this design [71], the

polarization controller adjustment was achieved by use of a feedback loop controlled by the DOP of the signal.

Ono *et al* [72] described another approach to first-order PMD compensation known as the PSP transmission method. It is a pre-compensation method in which a polarization controller is used to align the SOP of the input optical signal with either the fast or slow PSP of the fibre link. This method is not efficient since the control signal is tapped at the output of the fibre link and looped back to the input of the fibre. Depending on the length of the link, the loop may increase compensation time, hence making the compensator inefficient.

Other possible ways to compensate for the first-order PMD have been proposed, including the exploitation of planar lightwave circuits [73], electronics equalization [74] and high birefringence Bragg gratings [75-76].

3.4.2 Second-order PMDC

After eliminating the first-order PMD effect, the system performance is essentially limited by the residual higher order PMD [77]. Therefore, higher order PMD compensation is desirable. When the bit rate is increased above 10 Gb/s, the bandwidth of the signal becomes larger than the valid limit of first-order approximation, the so called PSP bandwidth [78]. In this case, the higher order PMD affects the various polarization and frequency components differently. In particular, as a result of second-order PMD, various spectral

components undergo a differential polarization change (depolarization), and a polarization-dependent chromatic dispersion (PCD) [79].

Several higher order PMDCs have been demonstrated and analyzed [81-91]. They are based on the principle that higher order PMDC can be achieved through the cascade of first-order PMDCs as shown in Fig. 3.4. The greater the number of stages, the more accurate the compensation; however, the high number of DOF also increases the complexity of the system while lowering the response time. This can be a problem because if there are fast changing SOPs in the link, the compensator may not be able to track the SOPs.

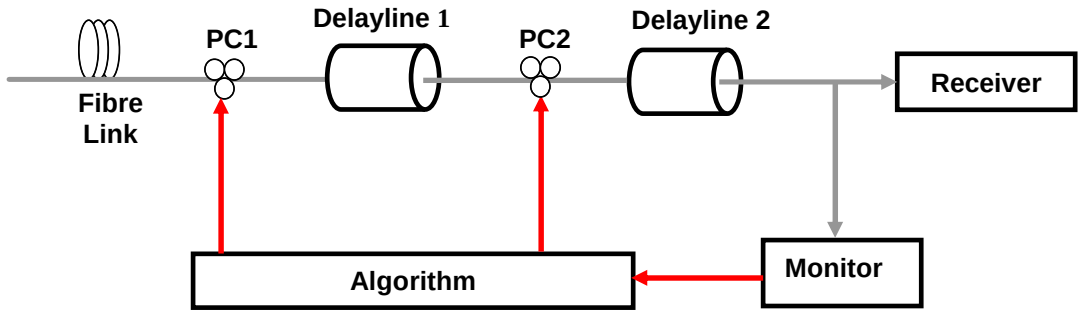

Fig. 3.4: Block diagram of two stage compensator for compensation of first- and second-order PMD.

The feedback configuration suffers from slow response time since it requires dithering of the signal to find the optimal point [58]. On the other hand, the feedforward configuration does not require dithering and its response time is fast, but requires polarization scrambling at the transmitter end. Feedforward technique is based on determining the PSPs of the fibre link and aligning them to the axis of the delayline using the polarization controller. For a fixed

single input SOP, one polarimeter measurement is not sufficient to determine the PSPs. Therefore, polarization scrambling is necessary to acquire multiple polarimeter measurements at the output of the fibre link at various input SOPs.

One of the first PMD compensators based on the feedforward control technique was reported by Rosenfeldt *et al* [91]. In this demonstration, the SOP of an optical source was scrambled at the input of the fibre, and the continuous DGD monitoring was realized by a polarization-resolved evaluation of the DOP. By making use of a lookup table, the DGD value was inferred and fed forward to a variable delayline in order to set the appropriate parameters for the compensator. The feedforward compensation technique based on PSP characterization and realignment was also demonstrated in Ref [92-93]. In this case the fixed delayline was used and by measuring the DOP and SOPs at the receiver end, the orientation and magnitude of the PSPs were determined. L. S. Yan *et al* [94] took this idea one step further and proposed a feedforward PMD compensator comprising a two polarization scramblers, one at the input of the link to scramble the input SOPs and another one at the end of the fibre link followed by the polarization dependent loss element. The measured RMS power fluctuation value through the PDL element was used as a control signal to the compensator. The analysis showed that this configuration is capable of compensating for PMD in a WDM system, in which an optical filter can scan across the entire wavelength range.

The use of a multistage compensator is another interesting idea that has been proposed. For example, Miao *et al* [95] reported a feedforward PMD compensator with four DGD elements and four polarization controllers. The required rotation matrix of the PCs was analytically determined, and Monte Carlo simulation was used to investigate the robustness of the compensator. The scheme proposed may not be practically workable because of the seven degrees of freedom.

With the introduction of WDM systems, where many channels are launched into the fibre, and compensation at channel level is need, the first- and second-order PMDC are inadequate. This leads to the next section where Multichannel PMDC will be reviewed.

3.4.3 Multichannel PMDC

Most of the PMD compensation of the low-order (first- and second-order) PMD that have been discussed above are restricted to low power signals. However, as the bandwidth of telecommunication systems and transmission distance increases, all-order PMD effects become increasingly important. In addition, nonlinearities caused by high optical power in channels, makes the PSPs power dependent, therefore making it impossible to use first-order PMD compensators in multichannel systems [96].

The feasibility of using a single compensator to compensate several channels at the same time was investigated and experimentally tested by Khosravani *et al* [97]. The technique was based on compensating for the worst-performing

channel at any given time and did not require demultiplexing of the channels. The multichannel optical equalizer mitigating intersymbol interference for 40 Gb/s NRZ signals was also demonstrated [98]. The authors made use of the two single-mode connected Mach-Zehnder interferometers (MZIs), where the amplitudes and phases of the two satellites were adjusted by varying the coupling ratios of the MZIs' adjustable input and output couplers as well as fine-tuning the path-length difference in each MZI. However, the drawback to single-mode-connected MZIs is that they have an intrinsic loss which could lower the efficiency of the compensator. Song *et al* [65] demonstrated a multi-channel PMD compensation based on the average DOP of all the channels as the monitoring signal; it was used to compensate for four 10 Gb/s channels for both non-return-to-zero (NRZ) and return-to-zero (RZ) modulation formats. Averaged-DOP technique could not work well because some channels are depolarized where at first were polarized.

CHAPTER 4

NONLINEAR EFFECTS IN OPTICAL FIBRE

A good understanding of the causes and effects of nonlinearities on the polarization state in wavelength division multiplexing (WDM) channels is required before tackling the challenges of compensating for PMD and nonlinear birefringence simultaneously. After the introduction to WDM, we give a brief review of the origin of nonlinear birefringence. An overview of the mathematical representation of the pulse propagating in a fibre carrying high intensity is presented. A review of the nonlinear polarization evolution in birefringent fibres then follows. The interaction of linear and nonlinear polarization rotation is also reviewed. Lastly, the work done on the effects of XPM polarization fluctuations on PMD compensation is reviewed.

4.1 Wavelength Division Multiplexing

In the early years, field-deployed systems were limited to transmitters and receivers at the two ends of the optical fibre communication link, which is known as a *standard simplex point–to-point optical link* [99]. This is illustrated in Fig. 4.1(a). In order to increase the number of signal carriers using simplex links, the signals from different light sources are used with separate and uniquely assigned optical fibres, as illustrated in Fig. 4.1(b). This arrangement is called *spaced-division multiplexed link*. With the development of distributed feedback (DFB) laser sources having defined wavelengths [100], and filters

that combine and separate closely spaced wavelengths [101], one can use independent and appropriately spaced wavelengths to send many channels over the same fibre, as illustrated in Fig. 4.1(c).

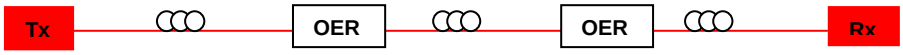

(a) 2.5 Gb/s

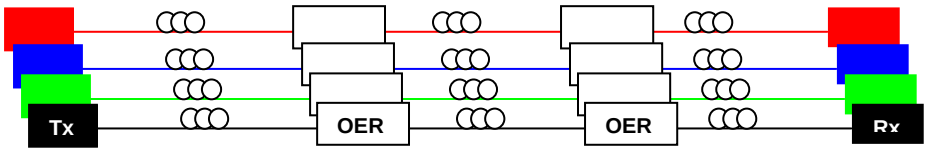

(b) 4 x 2.5 Gb/s

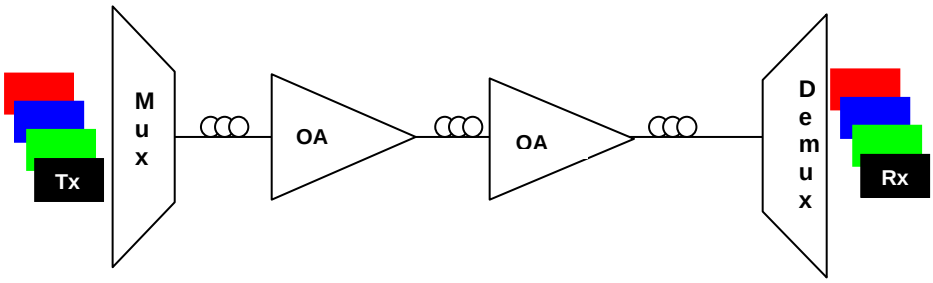

(c) 4 x 2.5 Gb/s

Fig. 4.1: (a) Standard simplex point–to-point optical link consisting of three optical fibre links separated from each other by optoelectronic regenerators (OER). (b) space-division-multiplexed link using 2.5 Gb/s transmission in four separate fibres. (c) introducing WDM achieves the same capacity as in (b) but with only one fibre link [102]. OA: optical amplifier.

WDM started playing a major role in telecommunications networks in the early 1990s. This resulted from the surge in demand for high-capacity links and the limitation of the installed fibre plant in handling high-rate optical signals over any substantial distance [103]. WDM therefore is more cost-effective; this most important advantage comes because instead of a large number of

electro-optic regenerators, a small number of optical amplifiers are used. If more channels are to be added and if there is a need to upgrade to higher bit rates, WDM has an edge over other systems because there is no need to install new fibres. Hence WDM is the choice that gives additional cost advantages.

The enabling technology for the cost-effective implementation of WDM was the creation and improvement of various passive and active optical components used to combine, distribute, isolate, and amplify optical powers at different wavelengths. The key enabler was erbium-doped fibre amplifier (EDFA) [104]; it has an ability to amplify multiple optical signals at different wavelengths.

The use of WDM enables one to achieve higher capacity transmission. Several channels can be multiplexed in an optical fibre. All channels are equally spaced in the spectral (frequency) domain by a parameter called channel spacing, which is the minimum frequency separation between channels that is required to guarantee minimum crosstalk degradation. The efficiency of the multiplexing can be defined by the ratio [105]:

$$\text{Spectral efficiency} = \frac{\text{Channel bit rate}}{\text{Channel spacing}}$$

The frequency grid, with a reference fixed at 193.1 THz (1552.52 nm), supports a variety of channel spacing ranging from 12.5 GHz to 100 GHz and wider. This is according to ITU-T standardization recommendation [106].

The two major hindrances to upgrading the WDM systems to 10 Gb/s and above are optical nonlinearities [107] and polarization mode dispersion [108]. In the following section we shall consider the nonlinearities in detail.

4.2 Origin of nonlinear Birefringence

Since the discovery of intensity-dependent change in the refractive index of a medium by Maker *et al* [109], it has been well known that the self-induced nonlinear birefringence in an optical Kerr medium leads to ellipse rotation, i.e. intensity-dependent rotation of elliptically polarized light. In its simplest form, the refractive index n' can be written as [99]

$$n' = n_0 + \underbrace{n_2 \frac{P}{A_{eff}}}_{\substack{\text{nonlinear} \\ \text{contribution}}}$$

where n_0 is the linear refractive index, n_2 is the nonlinear-index coefficient, A_{eff} is the effective core area of the medium and P is the optical power inside the fibre. The intensity dependence of the refractive index leads to a large number of interesting nonlinear effects; the most widely studied due to their negative effect on the signal in a WDM system are self-phase modulation (SPM), cross-phase modulation (XPM) and four-wave mixing (FWM) [110]. Nonlinear fibre optics play an increasingly important role in the design of high-capacity lightwave systems. The example is where the fibre lasers can be mode locked using the intensity-dependent change in the state of polarization (occurring because of SPM and XPM) when the orthogonally polarized components of single pulse propagates through the optical fibre [111].

4.3 Pulse-Propagation Equation

When considering wavelength-division multiplexing to increase the capacity of a fibre link, there are two nonlinear effects which impair transmission quality: cross phase modulation (XPM) and four-wave mixing (FWM). The extent to which they affect transmission quality depends on the relative polarization of the individual wavelength channels.

Based on Ref. [110], the propagation equations for the two principal polarizations in birefringent media can be obtained by factoring out the transverse dependence of the electric field components E_x and E_y:

$$E(\mathbf{r}, t) = F(x,y)A(z,t)\exp(i\beta_0 z) \tag{4.1}$$

where F describes the spatial distribution of the single fibre mode, A is the (slowly varying) amplitude envelope and β_0 is the propagation constant. Making allowance for PMD (including polarization mode coupling) and PDL, the slowly varying amplitudes, A_x and A_y, are described well by the following set of two coupled stochastic nonlinear Schrödinger equations [112]:

$$\frac{\partial A_x}{\partial z} + \beta_{1x}\frac{\partial A_x}{\partial t} + \frac{i\beta_2}{2}\frac{\partial^2 A_x}{\partial t^2} + \frac{\alpha_x}{2}A_x - \frac{1}{6}\beta_3\frac{\partial^3 A_x}{\partial t^3} + i\kappa(z)A_y e^{-i\Delta\beta_0 z}$$
$$= i\gamma\left(|A_x|^2 + \frac{2}{3}|A_y|^2\right)A_x + \frac{i\gamma}{3}A_x^* A_y^2 e^{-2i\Delta\beta_0 z} \tag{4.2a}$$

$$\frac{\partial A_y}{\partial z} + \beta_{1y}\frac{\partial A_y}{\partial t} + \frac{i\beta_2}{2}\frac{\partial^2 A_y}{\partial t^2} + \frac{\alpha_y}{2}A_y - \frac{1}{6}\beta_3\frac{\partial^3 A_y}{\partial t^3} + i\kappa(z)A_x e^{-i\Delta\beta_0 z}$$
$$= i\gamma\left(|A_y|^2 + \frac{2}{3}|A_x|^2\right)A_y + \frac{i\gamma}{3}A_y^* A_x^2 e^{-i\Delta\beta_0 z} \tag{4.2b}$$

where $\kappa(z)$ is the random mode coupling coefficient, $\Delta\beta_0$ is the birefringence parameter, α_x and α_y are the losses for the two polarization modes and the nonlinear parameter γ is given by

$$\gamma = \frac{n_2 \omega}{c A_{eff}} \tag{4.3}$$

The average loss is given by $\alpha = (\alpha_x + \alpha_y)/2$, while $\Delta\alpha = \alpha_x - \alpha_y$ represents the polarization dependent loss (PDL) in the link.

The last term on the right-hand side of the equations 4.2 is due to coherent coupling between the polarization components and leads to degenerate four-wave mixing (FWM). However, if the fibre length is much larger than the beat length L_B from equation (2.10), such as is considered here, it changes signs often and averages out to zero. Therefore it can be neglected.

If we assume that the fibre is linearly birefringent we can neglect mode coupling; PDL and third-order dispersion β_3 can be neglected too since β_2 is not equal to zero. The reduced equations become

$$\frac{\partial A_x}{\partial z} + \beta_{1x}\frac{\partial A_x}{\partial t} + \frac{i\beta_2}{2}\frac{\partial^2 A_x}{\partial t^2} + \frac{\alpha_x}{2}A_x = i\gamma\left(|A_x|^2 + \frac{2}{3}|A_y|^2\right)A_x \tag{4.4a}$$

$$\frac{\partial A_y}{\partial z} + \beta_{1y}\frac{\partial A_y}{\partial t} + \frac{i\beta_2}{2}\frac{\partial^2 A_y}{\partial t^2} + \frac{\alpha_y}{2}A_y = i\gamma\left(|A_y|^2 + \frac{2}{3}|A_x|^2\right)A_y \tag{4.4b}$$

The first term on the right-hand side in the brackets represents the self-phase modulation (SPM). The second term represents the cross-phase modulation (XPM).

4.4 Nonlinear effects.

The nonlinear effects occurring inside optical fibre limit the maximum power levels that can be carried by a pulse. They also affect the performance of long-haul WDM lightwave systems. This section focuses on the three major nonlinear phenomena namely SPM, XPM and FWM.

4.4.1 Self-Phase Modulation

SPM refers to the self-induced phase shift experienced by an optical field during its propagation in the fibre. SPM is responsible for spectral broadening of pulses [113] as illustrated in Fig. 4.2 and the formation of optical soliton in the anomalous-dispersion regime of fibres [114].

The SPM-induced spectral broadening is a consequence of the time dependence of nonlinear phase shift. This can be understood by noting that a temporally varying phase implies that the instantaneous optical frequency differs across the pulse from its central frequency. The time dependence of $\Delta\omega$ is referred to as *frequency chirping*.

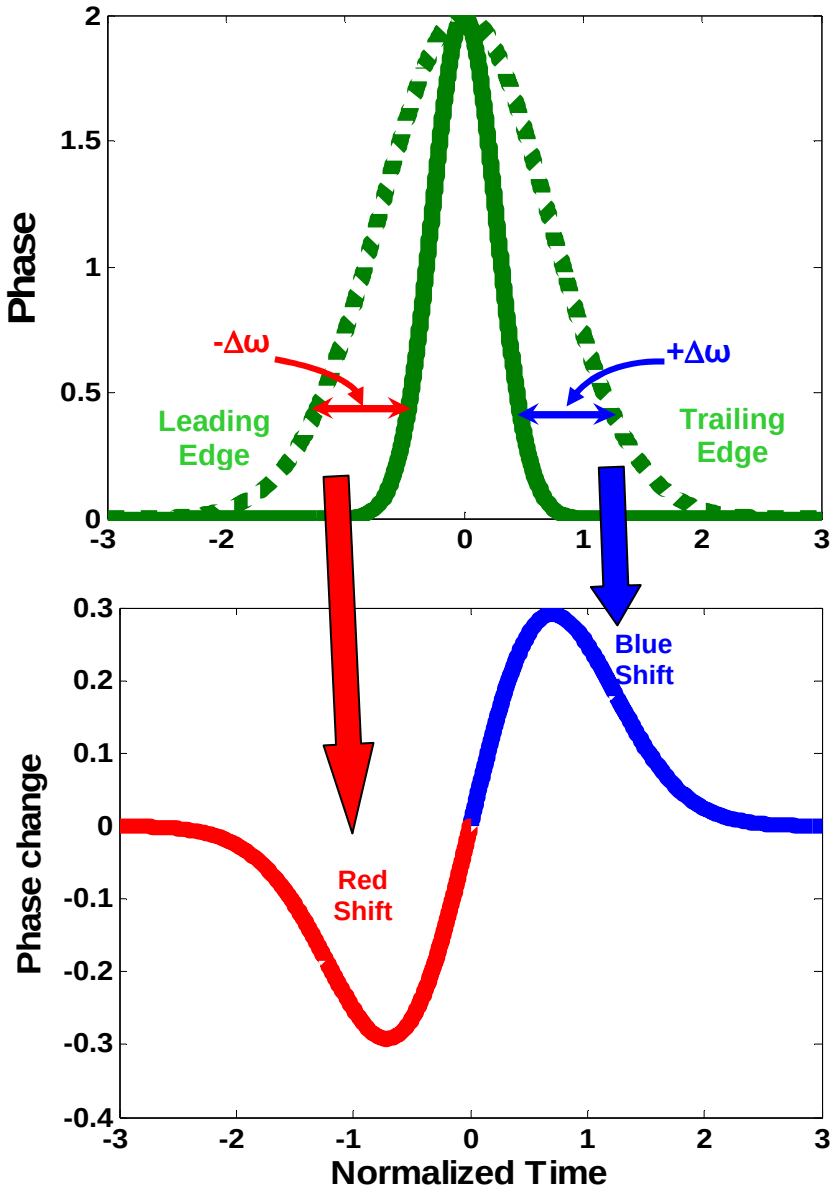

Fig. 4.2: Effect of SPM on broadening the ultra-short pulses. The green dotted line shows the broadened pulse; the green continuous line is the original ultra-short pulse.

The temporal variation of the induced chirp $\Delta\omega$ has two interesting features. First, $\Delta\omega$ is negative near the leading edge (red shift) and becomes positive near the trailing edge (blue shift) of the pulse. Second, the chirp is linear and positive (up-chirp) over a large central region of the pulse.

4.4.2 Cross-Phase Modulation (XPM)

In WDM systems, the intensity-induced refractive index gives rise to cross-phase modulation (XPM), which converts power fluctuation in a particular wavelength channel to phase fluctuations in other co-propagating channels [115]. The induced phase shift is due to the *walkover* effect, whereby two pulses at different bit rates or with different group velocities walk across each other [110]. As a result, the slower pulse sees the walkover and induces a phase shift. This implies that XPM broadens a weak pulse in the presence of a strong pulse. The total phase shift depends on the net power of all the channels and the channel spacing. XPM-induced power fluctuation is less pronounced as the channel spacing increases [116] and the total phase shift also depends on the bit patterns of all the other channels [117].

4.4.3 Four-wave mixing (FWM)

When three intense lightwaves of different frequencies (ν_i, ν_j, ν_k) are input to an optical fibre, additional frequencies are generated through the four-wave mixing (FWM) process due to the third-order nonlinearity [110]. The generated fourth signal is given by [99]

$$\nu_{ijk} = \nu_i + \nu_j - \nu_k \qquad \text{with } i, j \neq k \tag{4.5}$$

As an illustration Fig. 4.3 shows two waves at frequencies ν_i and ν_j.

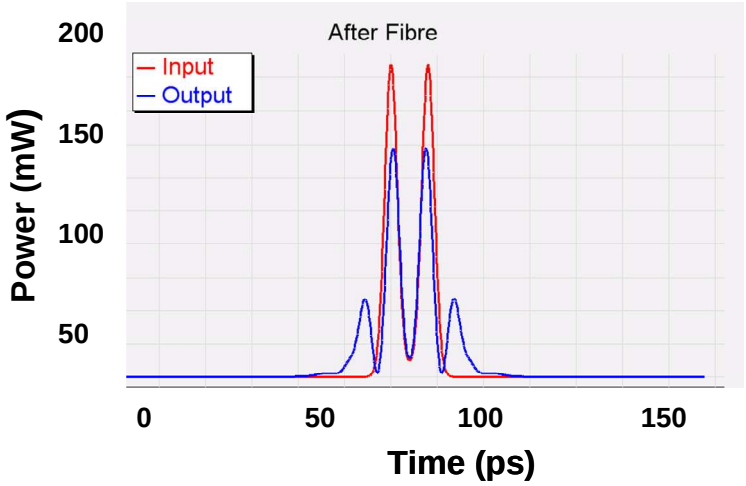

Fig. 4.3: Two frequencies interacting in the fibre generated two more frequencies.

In the case of equally spaced channels, new frequencies coincide with the existing frequencies and produce in-band crosstalk. Hill *et al.* [118] investigated the FWM process theoretically and experimentally in a single-mode fibre. Through a FWM process, three input waves with different frequencies generate nine new waves resulting from frequency mixing. Shibata *et al.* [119] showed the phase-mismatching effect in FWM efficiency in a single-mode fibre. The authors showed that the region of the frequency separation for satisfying nearly perfect phase matching extends over 50-120 GHz at the zero chromatic dispersion wavelengths. FWM through newly generated frequencies may degrade system performance in optical multichannel transmission [120]. From [121], it was observed that when all the lasers were modulated, crosstalk was observed at all frequencies between the two adjacent channels. It was concluded that FWM crosstalk becomes significant when the signal powers exceed 0 dBm/channel in a 10 GHz-spaced, 100-channel system using 1.5-pm sources and a single-mode fibre.

Thus, the successful design of high-capacity OFDM systems must include careful consideration of possible FWM interactions in the transmission fibre. Since the dispersion-shifted fibre is no longer being used for data transmission, FWM is not much of an issue in communication systems.

4.5 Nonlinear polarization evolution in birefringent fibre

The nonlinear interaction in WDM systems induces a nonlinear polarization scattering in one optical channel whenever there is high optical power present in the other channel. This leads to a power dependent change of the state of polarization. When analyzing nonlinear polarization evolution, two co-propagating channels are considered having arbitrary polarization. If the slowly varying envelopes of the fields for the two channels are denote by $\vec{A}_a$ and $\vec{A}_b$, their evolution in the fibre can be described by the equation [122]:

$$-i\frac{\partial \vec{A}_a}{\partial z} = \frac{8}{9}\gamma\left\{\left(\vec{A}_a^{+}\ \vec{A}_a\right)\vec{A}_a + \left(\vec{A}_b^{+}\ \vec{A}_b\right)\vec{A}_a + \left(\vec{A}_b^{+}\ \vec{A}_a\right)\vec{A}_b\right\} \tag{4.5}$$

where $\vec{A}^{+}$ is the transpose of A.

By neglecting PMD and PDL, it can also be shown, that no polarization evolution takes place between orthogonally polarized signals. This can be understood from Ref. [122] which showed that the rate of change of Stokes vectors $\vec{S}_a$ and $\vec{S}_b$ of the two channels along the z-axis is given by:

$$\frac{\partial \vec{S}_a}{\partial z} = \frac{16}{9}\gamma P_0\left(\vec{S}_a \times \vec{S}_0\right) \text{ and } \frac{\partial \vec{S}_b}{\partial z} = \frac{16}{9}\gamma P_0\left(\vec{S}_b \times \vec{S}_0\right) \quad (4.6)$$

where $\vec{S}_a$ and $\vec{S}_b$ represent the Stokes vectors of the two channels, P_0 is the optical power, and the average vector of $\vec{S}_a$ and $\vec{S}_b$, is $\vec{S}_0 = ½ (\vec{S}_a + \vec{S}_b)$. Equation 4.6 indicates that the Stokes vectors of two signals rotate at the same rate about the vector $\vec{S}_0$. This is illustrated in Fig. 4.3.

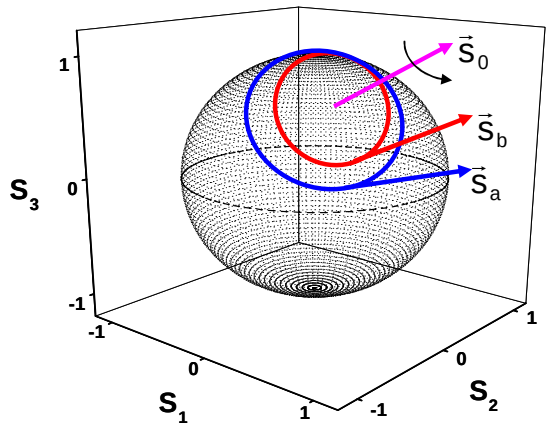

Fig. 4.3: Output Stokes vectors of two fields $\vec{S}_a$ and $\vec{S}_b$ as they precess around the stationary vector $\vec{S}_0$.

The magnitude of the vector $\vec{S}_0$ (P_m) depends on the fixed relative polarization angle θ between the probe and pump and the peak powers of probe (P_s) and the pump (P_p) respectively according to the equation [123]:

$$P_m = \sqrt{P_s^2 + P_p^2 + 2P_sP_p\cos\theta} \quad (4.7)$$

According to equation 4.7, the channel with the dominant power remains fixed, since its Stokes vector is almost coincident with $\vec{S}_0$. Therefore the output Stoke vector of the probe channel is guided by the relative angles between the pump and probe input SOP vectors and the magnitude of the pump power. The probe signal is highly depolarized if the input pump power is high and also if the input SOP vectors of the pump and probe are perpendicular to one another in Stokes space. But the signal remains polarized if the input SOP vectors are anti-parallel or parallel, regardless of the input pump power. This is demonstrated in our results in section 5.1.

It was reported further that the nonlinear polarization rotation resembles a conventional circular birefringence, in that it rotates SOP around S_3 on the Poincaré sphere but it differs significantly from the conventional circular birefringence in that it rotates the polarization ellipse in different directions depending on the SOP of the signal itself [124]. In addition, Vinegoni *et al* [125] in their work reported that the rotation direction of the nonlinear birefringence is different for the upper and lower hemisphere of the Poincaré sphere contrary to linear birefringence.

Wang *et al* [126] investigated the evolution of the degree of polarization of individual channels and their Stokes parameters in WDM systems in which the Kerr nonlinearity and chromatic dispersion are accounted for while the PMD and PDL are negligible. Furthermore, the report states that the presence of nonlinearity and chromatic dispersion can lead to channel

interaction such that they cause *repolarization when the channels are closely spaced*. This reduces the efficiency of PMDC.

Since the linear SOPs rotate around S_1 while the nonlinear SOPs rotate around S_3, it would be interesting to explore how the linear and nonlinear effects influence the state of polarization evolution. The following section reviews the work done on evolution of linear and nonlinear polarization in a fibre.

4.6 Interaction of linear and nonlinear polarization rotation

At low intensities, the linear birefringence causes polarization fluctuations which produce linear signal pulse distortion known as linear PMD, which has been extensively studied as outlined in section 2.3. As the distance of transmission continues to increase, the signals carrying high intensities also need to increase in order to reduce the number of repeaters and amplifiers along the link. Under these conditions, in addition to linear birefringence, the intensity induced-birefringence known as *nonlinear birefringence* is developed in the fibre. The power dependent polarization fluctuation is produced causing the intensity dependent signal pulse distortion known as *nonlinear PMD* [127].

Analytical work has extensively been done on nonlinear birefringence coupling on PMD. For example Shi *et al* [128] investigated the nonlinear interaction of a birefringence optical fibre with consideration of both the linear and birefringence fluctuation and polarization mode dispersion. In their work

they showed that the linear random mode coupling between the two polarization modes plays a very important role in the stability of the soliton transmission for soliton based optical fibre communication. Wai *et al* [129] established that nonlinear PMD exists whenever there is high intensity carried by the signals and its effect will affect very high data rate systems operating at near 100 Gb/s. These authors further stated that reducing the linear PMD by decreasing the decorrelation length reduces the mixing on the Poincaré sphere which in turn increases the nonlinear PMD.

The numerical study of the coupling between linear orthogonal modes due to nonlinear polarization evolution has been carried out where it was concluded that the interaction between the linear and nonlinear birefringence causes the successive and periodic energy exchange between the fast and slow linear modes of the fibre [130]. Models have been developed that describe the interaction between XPM, PMD and PDL [131]. It showed that XPM changes the direction of the polarization but does not affect the DGD. This point has been dealt with experimentally in our work in Chapter 5. Effects of nonlinearities on PMD have been reported both experimentally [132] and theoretically [133].

Unfortunately in all these investigations reported in this section there is little mentioned about the experimental work where the effect of mode coupling has been considered. Most investigators assumed that mode coupling is negligible. This has been one of the focus of our project as outlined in our result section in chapter 5.

4.7 Effects of XPM polarization fluctuations on PMD compensations

Since the random nonlinear birefringence rotates the SOP differently from the linear birefringence, and at high intensity the PSPs are power dependent, it will be impossible to fully compensate for first-order PMD. This is because the first-order PMD compensation technique is solely dependent on the alignment of the PSPs from the fibre output with the axis of the DGD delay line.

Khosravani *et al* [134] has demonstrated both numerically and experimentally the effect of XPM-induced PSP rotation on first-order PMD compensator. The author showed that the nonlinear phase change due to XPM induces a bit-pattern-dependent change in the SOP that translates to uncertainty in PSPs. Statistical assessment of XPM impact on an optical PMD compensator was carried out [135]. The compensation efficiency was evaluated by measuring the difference between the Q-factor penalty with and without compensation. Effects of XPM-induced polarization fluctuation on first-order PMD compensators have been demonstrated. For example, Pan *et al* [136], used a probe-pump model to show the distortion caused by XPM on a compensated signal and in addition the authors proposed the bipolarization modulation as a solution to overcome the effects of the XPM on a compensated system. Lee *et al* [137], analytically and experimentally demonstrated that the performance of the WDM systems could be degraded by the optical Kerr effect and DGD crosstalk, even when first-order PMD is completely compensated.

CHAPTER 5

INTERACTION BETWEEN LINEAR AND NONLINEAR PMD

In single mode fibres, both the orientation of the principal birefringence axes and magnitude of the birefringence vary randomly with distance along the fibre according to the conditions given in section 2.3.2. Because the two principal polarization states have slightly different group velocities, these polarization fluctuations produce linear or intensity-independent signal pulse broadening and distortion, known as linear PMD. In addition to the linear PMD, at high intensities, power dependent polarization fluctuations produce nonlinear or intensity –dependent signal pulse distortion, known as nonlinear PMD. In this chapter we investigate the interaction between nonlinear and linear birefringence in optical fibre with consideration of polarization mode coupling.

5.1 Dependence of probe signal DOP on the orientation of pump signal SOPs

Fig. 5.1 shows the simulation and experimental setups that were used to investigate the effects due to interaction between nonlinear birefringence and linear PMD as the pump signal SOPs oriented through 180^{o}. Simulations were carried out using Virtual Photonics Inc (VPI) software [138].

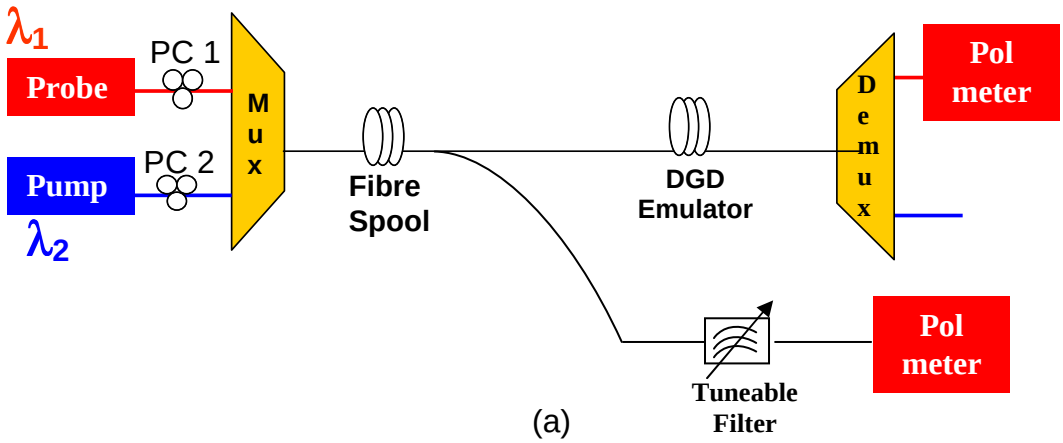

(a)

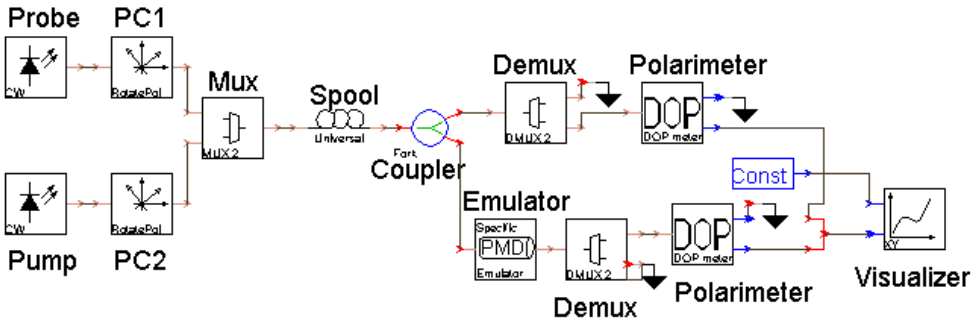

(b)

Fig. 5.1: Measurement setups used to investigate the dependence of probe signal DOP on the power and orientation of SOPs of the pump signal: (a) Experimental setup, (b) Equivalent VPI simulation setup. Mux: multiplexer, Demux: Demultiplexer

In both set-ups, the probe laser at a wavelength, λ_1, (=1551.72 nm) represented the channel suffering from cross-talk induced polarization fluctuation, while the pump laser at wavelength, λ_2, (=1552.12 nm) represented a nearby interfering channel. The channel spacing is thus 50 GHz (0.4 nm). Polarization controller, PC1 maximized the probe input power into the fibre, while polarization controller PC2 rotated the input pump SOPs with respect to the probe signal SOP. The pump signal was launched at powers of 3 dBm, 6 dBm and 13 dBm, and for each input power the pump signal SOPs were rotated through 180^{o} while observing the output DOP of the probe signal.

The two signals co-propagated through a 24 km long single mode fibre having a small PMD of 0.2 ps and therefore the effects of PMD were neglected. Using a coupler, part of the signal from the spool passed through an emulator before being demultiplexed and effects due to interaction between nonlinear birefringence and linear PMD on probe signal analysed by the polarimeter. The remainder of the signal from the coupler passed through a filter of bandwidth 0.3 nm, where the probe signal was filtered through and the effects of nonlinear birefringence alone on probe signal could be analyzed by the second polarimeter.

For simulations, the 24 km standard single mode fibre had a dispersion of 17 ps/nm-km, effective area of 80 μm^2 and the PMD of 0.24 ps. The PMD emulator was based on the model developed by Francia et al. [21]. This model was chosen mainly because the levels of differential group delay (DGD), polarization chromatic dispersion (PCD) and the depolarization rate are defined individually. Since the emulator is deterministic, it is possible to select specific combinations of first and second order PMD. This is particularly useful for examining worst-case PMD conditions, which have extremely low probabilities. The channel spacing, probe wavelength and pump wavelength were fixed at the same values as those in the experimental setup.

The emulators used in the experimental setup comprised of a small number of randomly concatenated sections of PM fibres. The first-order and second-order PMD statistics for the 10 and 24 segment emulators used in experimental measurements and simulations are shown in Fig. 5.2 (a) and (b)

respectively. In both cases, the DGD statistics follow a Maxwellian distribution that is characteristic of ideal emulators. The average DGD is nearly the same in both the 10 segment and 24 segment emulators, but the average SOPMD is larger for the 24 segment than for the 10 segment emulator. The experimental and simulation emulators have the same length for each segment and the number of mode coupling centres is the same in each case.

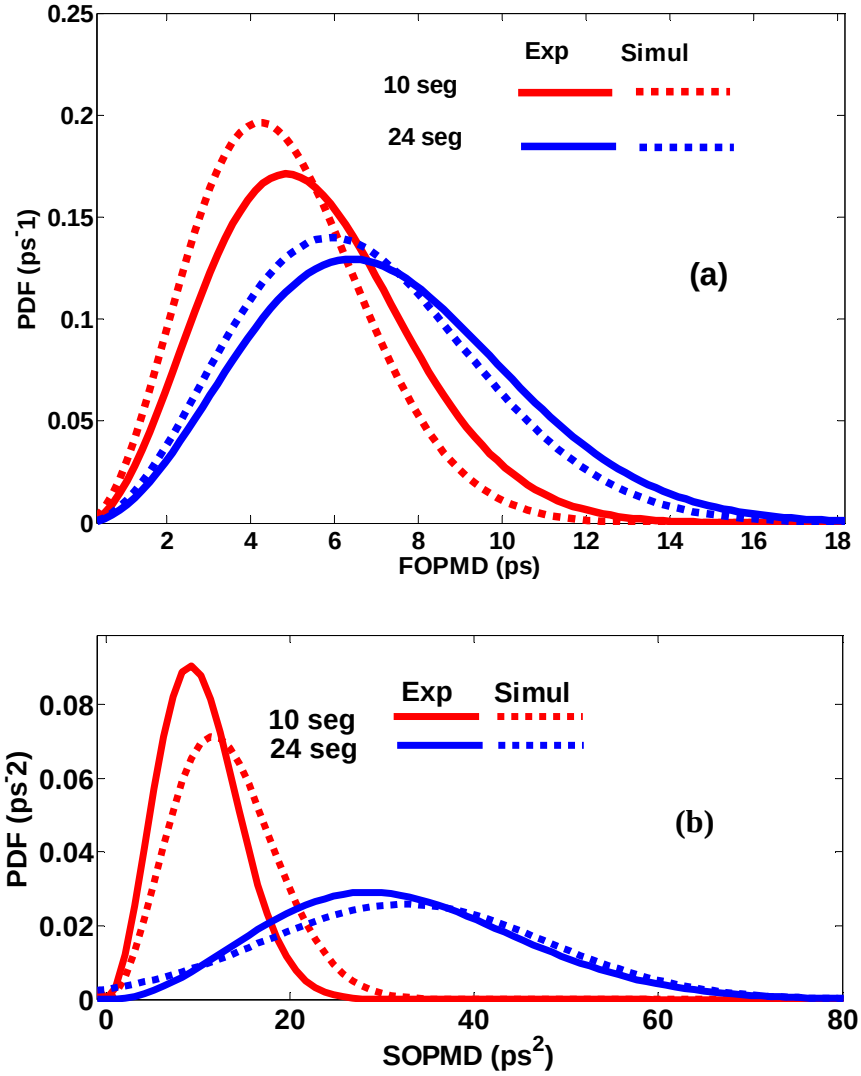

Fig. 5.2: Probability density functions of emulators for 10 segments and 24 segments. (a) First-order PMD; (b) second-order PMD. Exp: experimental, Simul: simulation

Rotation of the pump signal SOPs was found to have a high effect on the probe signal as the relative angles between SOPs of probe and pump signal

approached 90^o, but the probe signal is less affected when the relative SOPs are launched parallel (0^o) or anti-parallel (180^o) in Stokes space as indicated in Fig. 5.3 (a) and (b). When the input SOPs of the probe and pump signals were launched at 90^o from each other, the depolarization of the probe signal increased with increasing pump input power; however, if the launching angle was 0^o or 180^o, increasing the pump power did not affect the probe signal. This implied that the nonlinear birefringence penalty was high (low DOP) when the signal input SOPs in the two channels were perpendicular to one another in Stokes space (i.e. 45^o in Jones space). On the other hand, when the signal input SOPs were parallel or anti-parallel to each other in Stokes space (perpendicular in Jones space), the nonlinear birefringence penalty was very low. This is because at 90^o the power is coupled equally into the two birefringent axes, and therefore the interaction is strong but when the relative signal SOPs are parallel or anti-parallel to each other, there is weak interaction between the signals resulting in a minimal nonlinear birefringence effect.

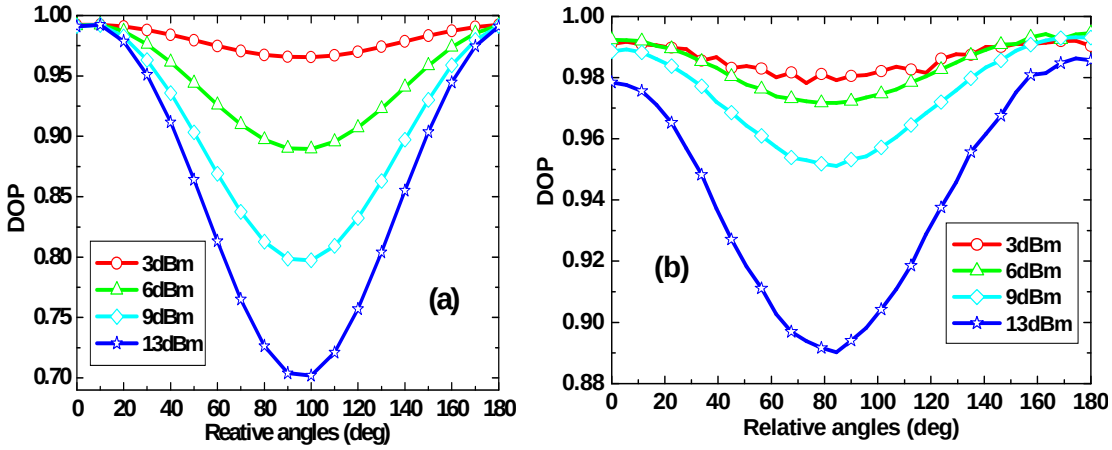

Fig. 5.3: Probe DOP variation with relative launch SOP angle for different pump powers in a 24 km spool. (a) VPI Simulation results and (b) Experimental results.

Fig. 5.4 shows the results of the probe signal DOP as a function of relative SOP angle in the presence of both linear and nonlinear PMD obtained using 10 and 24 segment emulators. The small difference between simulated and experimental results is attributed to the polarization dependent loss (PDL) of the optical devices that were used, which was not taken into consideration in the simulation. In addition, the emulator properties in experimental and simulations conditions might not be exactly the same.

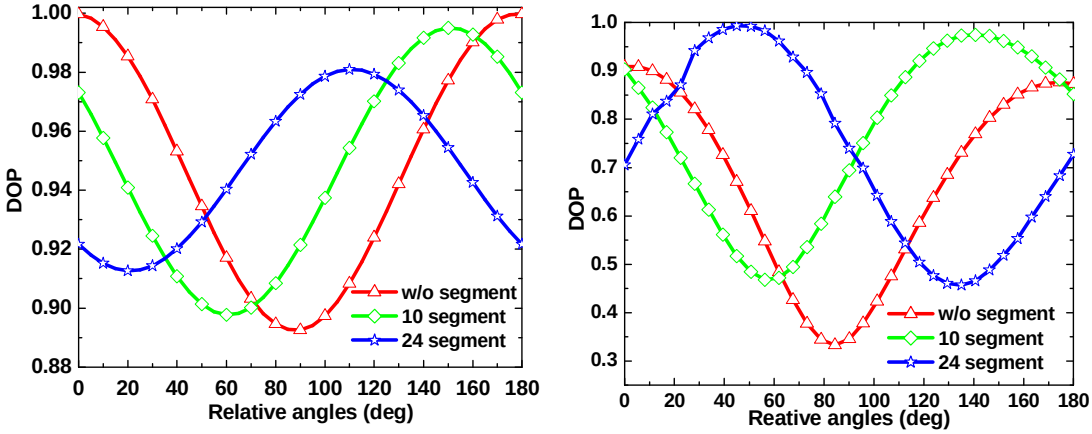

(a) (b)

Fig. 5.4: Probe channel DOP variation as a function of relative SOP angle between the signals in the presence of linear and nonlinear PMD, (a) VPI simulation results and (b) Experimental results. The power for the probe signal was 3 dBm and that for the pump signal was 13 dBm.

From the Fig. 5.4, it can be observed that the probe DOP variation was sinusoidal over the entire range of relative SOP angles. For example, in the case of the 10 segment and 24 segment links, the probe SOPs had gone through nearly one cycle, while in the spool (red) alone the SOPs had covered half a cycle. At 90^{o}, the DOP for the signal passing through the spool alone was low, while the DOPs of the signals passing through the 10 segments or 24 segments were relatively high. This was clear evidence that the linear

PMD rotated the SOPs in a different direction to nonlinear PMD. In general, we deduce that in systems where both nonlinear PMD and SOPMD exist, the DOP of the signal improves because the SOPMD cancels the nonlinear PMD.

When the probe signal and pump signal SOPs were launched anti-parallel or parallel to one another, the nonlinear PMD had no effect on the probe signal and SOPMD acted normally; it depolarized the signal.

5.2 Effect of nonlinear birefringence on first- and second-order PMD

To further support the analysis in section 5.1, the experiment was performed where the input power of the pump signal was varied as the DOP of the probe signal was monitored. The input probe signal power was kept constant at 3 dBm. As shown in Fig. 5.5(a), the DOP of the probe signal was measured as a function of the input pump power in the presence of nonlinear PMD alone (spool alone) and also in the presence of both nonlinear and linear PMD (spool and emulators). The histogram in Fig. 5.5(b) shows the average probe DOP taken over all the input pump powers for different links.

From Fig. 5.5(a) we observe that in links without mode coupling the DOP decreases with increasing input pump power. In the other words the nonlinear birefringence increases with the input pump power. Since the 24 km spool has low PMD, the relative states of polarization of the channels are preserved over a distance long enough for nonlinear interaction to occur. The nonlinear birefringence therefore breaks the degeneracy, rotates and scatters the SOPs over large angles. Similarly, in the case of the PMF, since the DGD and

PSPs are constant, we expect the SOPs that propagate along the two fixed birefringent axes to be preserved (in PMF fibre the birefringent axes are regarded as the PSPs). However, the nonlinear birefringence induced in the fibre axes randomizes the SOPs, causing the signal to remain depolarized.

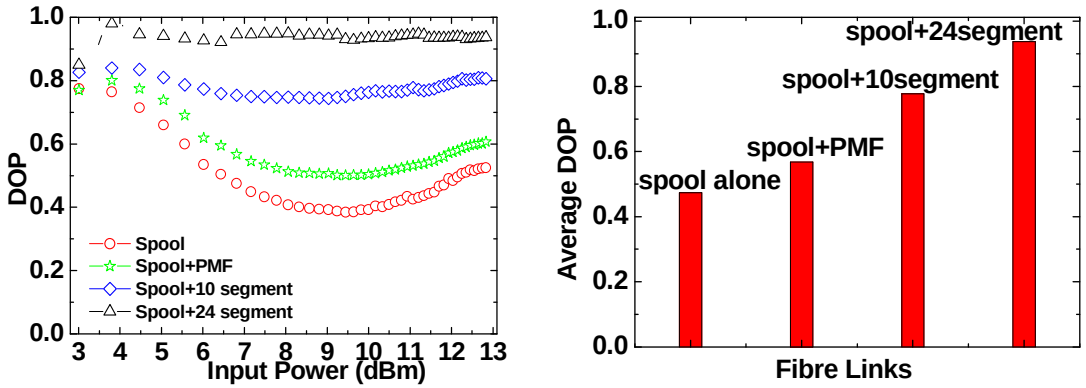

(a) (b)

Fig 5.5: (a) Measurements of the DOP of the probe channel as a function of the input power of the pump channel at different links. (a) Histogram of average DOP over all input pump powers for each link.

Nonlinear induced-birefringence was found to couple with SOPMD in such a way that the nonlinear polarization rotation effect between channels was reduced, as observed in Fig. 5.5(b), where the average probe DOP increased with increasing mode coupling centres. This was due to the fact that high SOPMD in the link caused the state of polarization of the probe channel to change quickly over a short distance and became uncorrelated. This led to the averaging of the nonlinear polarization rotation effects and a subsequent reduction in the nonlinear birefringence-induced variation of the principal states of polarization. This observation was further confirmed by results obtained from field measurements on two buried fibre links with low and high PMD at the Port Elizabeth Telkom exchange station as seen in Fig. 5.6. The

low PMD link had average DGD and SOPMD of 5 ps and 13 ps^2 respectively, while the high PMD link had 19 ps and 57 ps^2. Each link was of length 84 km.

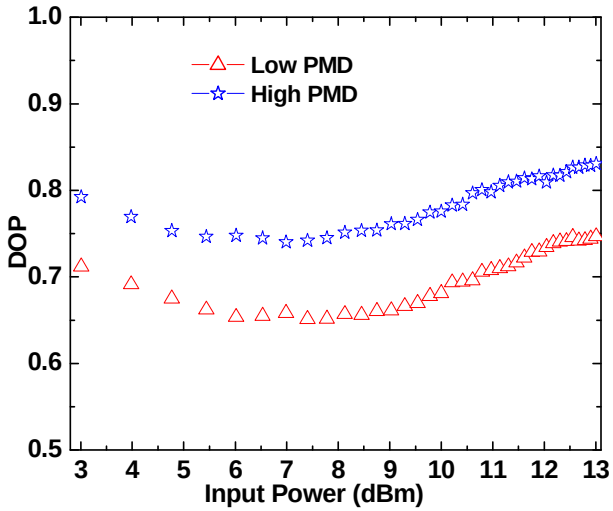

Fig 5.6: Variation of the DOP as a function of input power. Experiments were performed on two buried fibre links with low and high PMD at the Port Elizabeth Telkom exchange station.

Since the random birefringence in a fibre causes the output SOP vector to change, then the deviation or scattered angle measured between two output SOP vectors can be used as a measure of the birefringence effect. In Fig. 5.7 the total deviation angle measured with reference to the output SOP vector at 3 dBm was determined as the input pump power increased.

At low pump power (see the inset graph), the probe signal through the mode coupled link has its output SOPs scattered at larger angles than the output SOPs of the signal through either the low PMD link (spool alone) or highly birefringent fibre link (spool + PMF). Since the mode coupled link is modelled by large number of segments of fibres having random lengths and random fusion angles between segments [139], the output polarization vectors from the previous segment are resolved into new pairs of local PSPs belonging to

the next segment. The output SOPs are therefore randomly scattered. This can be traced as a random path on the Poincaré sphere.

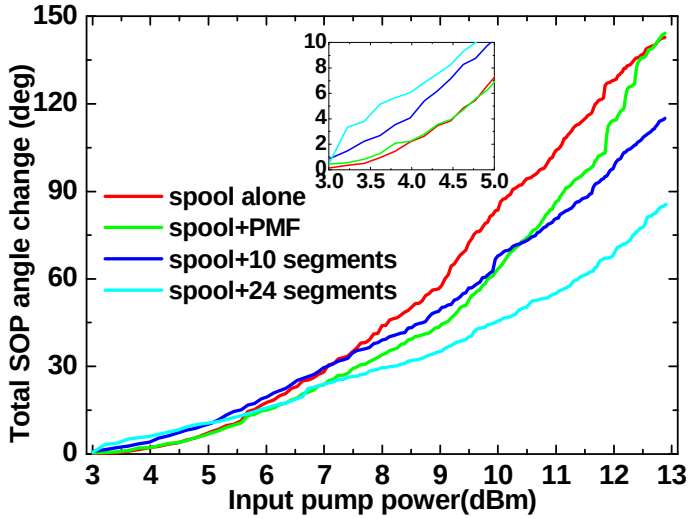

Fig 5.7: Total SOP angle change as a function of input pump powers

For a polarization-maintaining fibre (PMF) with constant birefringence, the two PSPs coincide with the two principal axes of birefringence of the fibre [17]. Therefore at low input pump power where the nonlinear birefringence is negligible, the polarization vector (with components resolved into the two axes) is preserved, thus the output SOP vector drifts only to a small extent from its initial position. But the two resolved vectors have a maximum or minimum group delay. In the low PMD regime, in principle there is low output SOP scattering because the linear and nonlinear birefringence in the fibre is negligible.

When the input pump power increases, there is an observable effect of the nonlinear birefringence on signal through all the three links. In the mode coupled link, since the nonlinear birefringence rotates the polarization vector

in the opposite direction to linear birefringence [132] it is probable that due to nonlinear birefringence effects the SOPs of the signal in one segment are rotated such that the PSP from the previous fast axis/slow axis is aligned with the slow/fast axis of the next segment. This reduces the resultant linear PMD vector, and yields the low scattering angles of the SOPs as observed in Fig. 5.7. Generally, the nonlinear birefringence vector may be added to or subtracted from the linear PMD vector [125]. Unlike the mode coupled link, high power launched into each of the two constant birefringence axes of the PMF link do change, creating nonlinear birefringence in each axis which rotates the resolved polarization vectors. Hence the resultant output SOP vector drift with large angle from the initial position. Therefore in non-mode coupled links the nonlinear birefringence induced in the link distorts the signal.

In summary, high SOPMD in the link which is due to mode coupling sometimes reduces the effect of nonlinear birefringence on the signal. In links with high FOPMD or no PMD at all, the nonlinear birefringence effects distort the signal. In addition, the nonlinear birefringence effects will rotate the PSPs only; they do not change much the DGD of the link.

5.3 Effect of nonlinear polarization rotation on the fast and slow PSP axes in the presence of PMD

Fig. 5.8 shows the setup used to investigate the effect of nonlinear birefringence on the fast and slow axes of the fibre link. The three WDM sources used were operating at 1551.72 nm (Upper Sideband: λ_{USB}), 1552.12 nm (Centre wavelength: λ_C) and 1552.52 nm (Lower Sideband: λ_{LSB})

respectively. Their respective input powers were 3 dBm, 13 dBm and 3 dBm and the channels spacing was 0.4 nm (50 GHz). This represented a symmetrical optical spectrum where the power falls off from the centre wavelength.

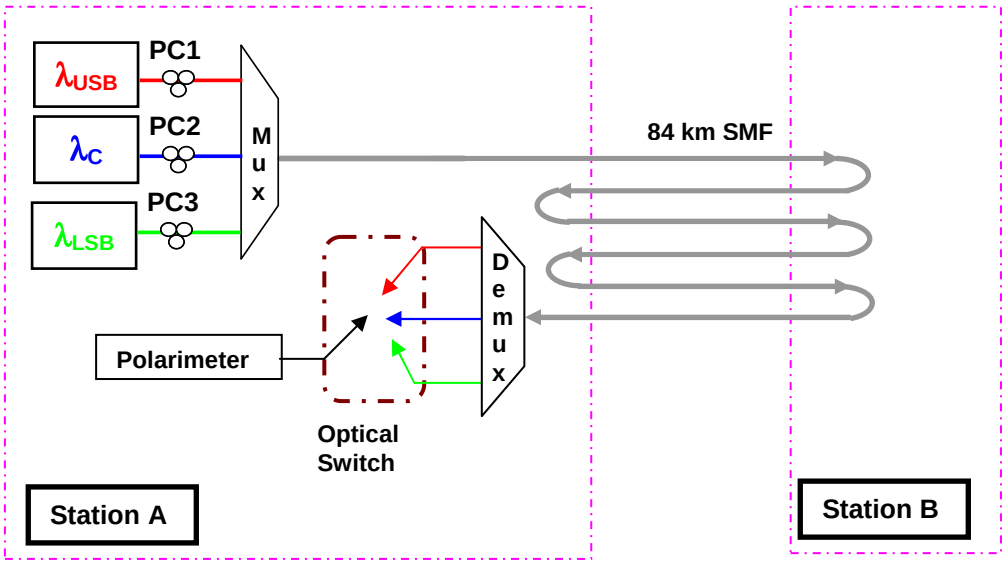

Fig. 5.8: The setup used to investigate the effect of nonlinear PMD on signals launched along the two fibre axes as the input power of the centre wavelength changes and when the SOPs of central wavelength are aligned at 0^o, 90^o and 180^o.

The polarization controller PC1 was used to align the SOPs of USB (SOP_{USB}) along the (0,0,1), the PC3 aligned the SOPs of LSB (SOP_{LSB}) along the (0,0,-1), while polarization controller PC2, was used to orientate the SOPs of the centre wavelength (SOP_C) at three angles: 0^o, 90^o and 180^o in the Stokes space with respect to (0,0,1). At each angle setting, the power of the centre wavelength was varied and, making use of a demultiplexer and optical switch, the DOP and SOPs for each channel were measured using a single polarimeter. The experiments was carried out on six looped buried fibres installed between two exchange stations in Port Elizabeth, South Africa, with a total transmission distance of 84 km. The average first- and second-order

PMD was 19 ps and 54 ps^2 respectively, measured over a wavelength range of 50 nm (1520 nm - 1570 nm).

Fig. 5.9 (a) shows the measured DOP of the upper sideband (USB) and lower sideband (LSB) signals as a function of input power when the SOP of the centre signal was aligned at 0^o, 90^o, 180^o with respect to (1,0,0). When SOP_C was aligned parallel to SOP_{USB} it was observed that the USB signal was less affected while the LSB signal decreased systematically. However, when SOP_C was aligned 90^o from the SOP_{USB}, both subcarrier signals' DOP did not change much, though we can still note some slight difference between them. The USB signal DOP (DOP_{USB}) was reducing with increasing input power, but after around 9.5 dBm, the DOP_{USB} started to improve, while the LSB signal DOP (DOP_{LSB}) slowly reduced with increase in power.

When SOP_C was aligned parallel to SOP_{LSB} (180^o), the DOP_{USB} drastically reduced with increasing input power up to 10 dBm, after which the DOP_{USB} started to increase, while the DOP_{LSB} remained nearly constant.

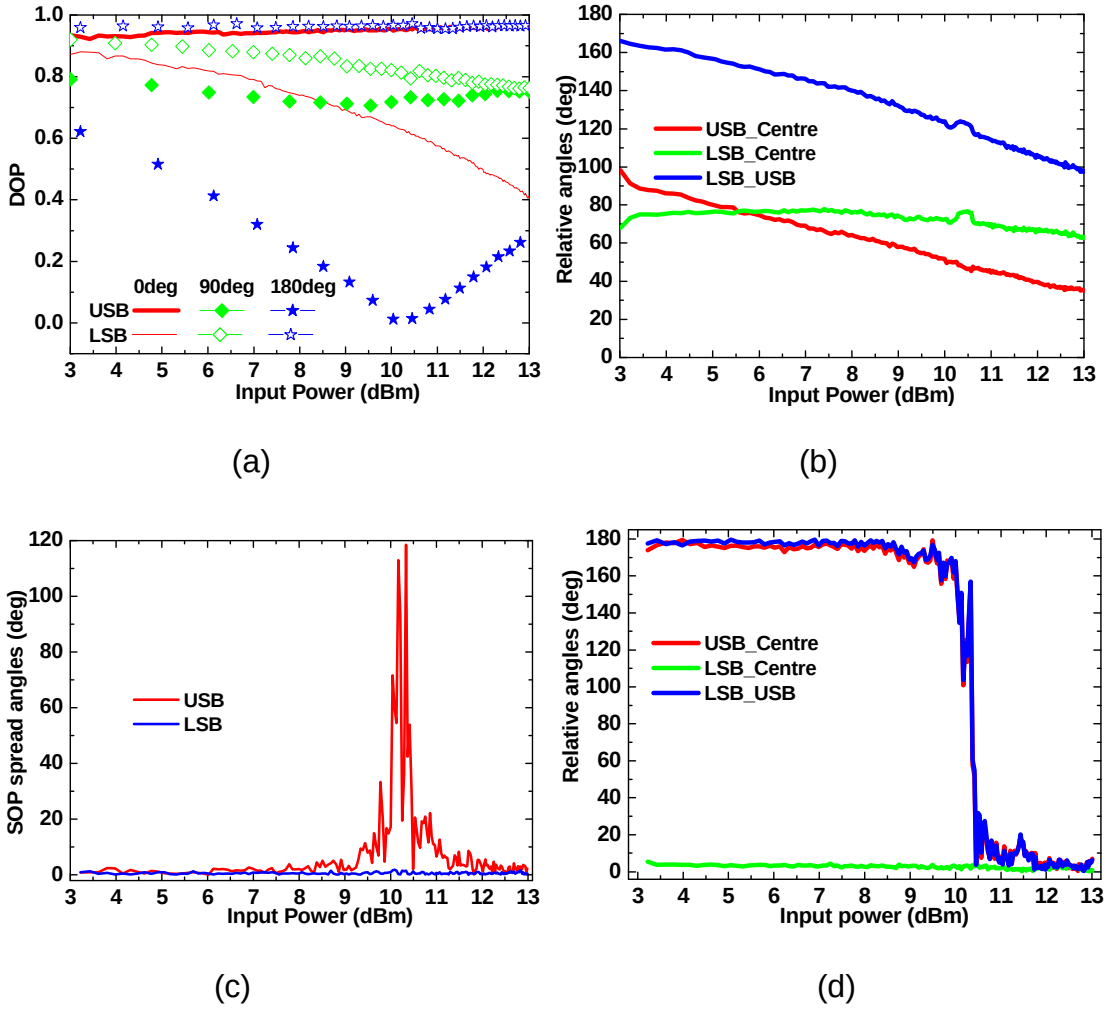

Fig. 5.9: (a) Measured DOP of LSB and USB signals with input power of the Centre wavelength, when the SOP vector of the Centre wavelength is aligned at 0^o, 90^o and 180^o with respect to the LSB SOP vector; (b) Variation of relative SOP angles as a function of input power when SOP_C was launched at 90^o from SOP_{USB}; (c) The spread of SOP_{USB} and SOP_{LSB} angles as a function of input power of the centre signal when the SOP_C is aligned 180^0 from SOP_{USB}; (d) The relative angles measured between SOP_{USB} and SOP_{LSB} as a function of input power of the centre signal when the SOP_C is aligned 180^0 from the SOP_{USB}.

From Fig. 5.9(a), at low power the slow rate of decline of the DOP of all signals shows that the SOPs of respective channels which were initially orthogonal did not interact much, leading to less scattering. This suggests that at low intensities, both axes are stable centres, and a linearly polarized input signal coupled into the fibre along either axis will preserve its polarization.

At high intensities, the nonlinear birefringence effect is strong, and the polarization evolution in the principal axes is drastically changed. It is observed that as the power increased, the nonlinear birefringence also increased and is added to the existing linear PMD. This is why the DOP_{USB} and DOP_{LSB} decreased with increasing power, as was shown in section 5.2. This was caused by the "SOP walk-off" or cross-polarization rotation as observed from Fig. 5.9(b) where the relative angles between the SOP of the three signals decreased with increasing input pump power. Decreasing relative angles indicates that there was an increasing interaction between the SOPs of the three signals which gave rise to polarization scattering, hence decreasing the DOP of the channels. Comparing Fig. 5.9(b) and (d), it is observed that the two birefringent axes are not equally excited. In Fig. 5.9(b) the SOP_C is aligned at 90^o implying that the pump power is equally launched into the two axes. The relative angles between the SOP_{LSB} and SOP_C are relatively constant (green line); this shows that the increasing pump power only weakly affected the axis along which the SOP_{LSB} vector was launched. Unlike the relative angles between the SOP_{LSB} and SOP_C, the relative angles between the SOP_{USB} and SOP_C decreased with increasing power (red line), indicating that the axis along which the SOP_{USB} was launched was highly affected by the power-induced birefringence. The same observation is made in Fig. 5.9(d) where the SOP_C was launched in the same direction as the SOP_{LSB} vector. Therefore the two birefringent axes are not equally excited. In the most excited axis, the nonlinear birefringence vector tends to rotate in such a way that it adds to the linear PMD vector. When two vectors are equal and parallel, there is a maximum polarization scattering as indicated by the

scattering angles in Fig. 5.9(c). Beyond this critical point, the induced nonlinear birefringence vector cancels the existing linear PMD vector, hence giving rise to the DOP improvement as shown in Fig. 5.9(a) (filled star). This could be attributed to the fact that the effective beat length due to addition or subtraction of linear and nonlinear birefringence is power dependent [140]. It is worthwhile to note from Fig. 5.9(d) that the output SOP_{USB} vector rotated with power through 180^{o}. This is a clear indication that PSPs rotate when the nonlinear birefringence is present in the optical communication systems**,** hence PSPs become power dependent.

5.4 Summary of results

The effect of nonlinear birefringence-induced polarization rotation on linear birefringence and mode coupling was investigated. It was shown that nonlinear polarization scattering in the probe channel depended greatly on the orientation of the pump channel polarization vector, as well as on the power carried in the pump channel.

It was also demonstrated that for low PMD links where the state of polarization is preserved, the nonlinear birefringence-induced polarization rotation effect randomizes the state of polarization thereby depolarizing the signal. In high PMD links where mode coupling is high, the nonlinear birefringence couples with second-order PMD in such a way that reduces the penalty and improves the signal DOP.

When nonlinear birefringence becomes significant, asymmetry arises between the two principal axes of the fibre, such that for the signal coupled along the fast axis, there exists a critical power above which the nonlinear birefringence cancels the linear birefringence. In fibre links with high PMD, it has been observed that this effect is not expected to be strong if the power is coupled equally into the two axes.

CHAPTER 6

DESIGN AND CONTROL OF A MULTICHANNEL PMD COMPENSATOR

This chapter starts with characterizing the first-order PMD compensator that was designed and built by the research group at Padova University, Italy. The project was a result of collaboration between Nelson Mandela Metropolitan University, South Africa and Padova University, Italy. These results form part of work that has been accepted for publication [141]. The first-order compensator results serve to illustrate methods that can be used to characterize the compensator. The sections that follow demonstrate a DOP-based multichannel PMD compensator using a feedforward method. The results from the laboratory and field tests showing the stability of the compensator are discussed in the last section.

6.1 Characterization of First-order PMD Compensator

Fig. 6.1 shows the experimental setup adopted during the characterization stage of the PMD compensation system. Light from a laser source passes through a polarization scrambler before it goes to the fibre link. A waveform generator is used to drive the polarization scrambler. A small part of the signal (1%) at the input of the polarization control (PC) board is tapped by a splitter and detected by the photodiode PD1 to keep track of the input power level. This is required in order to allow the control algorithm to discern

between power fluctuations due to PMD from those due to input power variations.

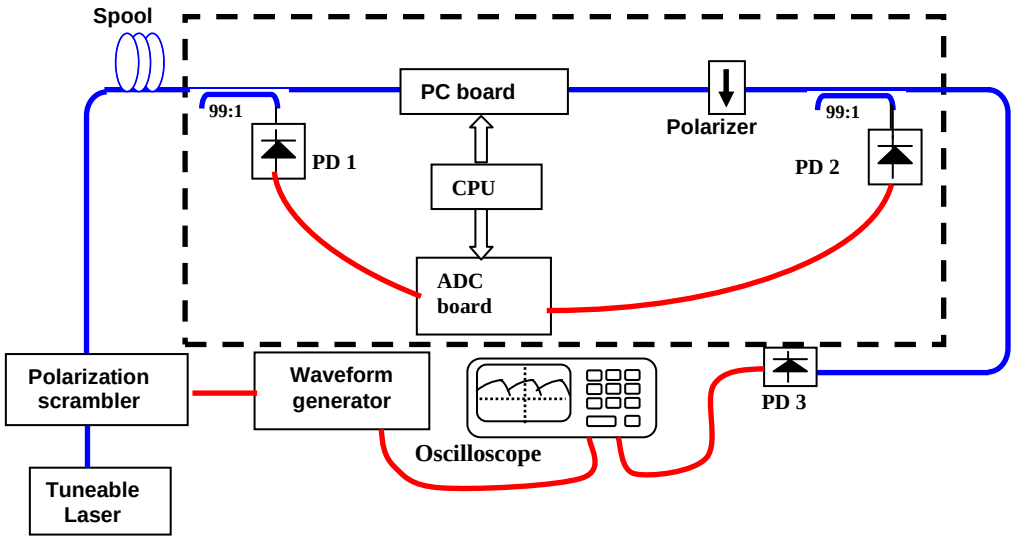

Fig. 6.1: The functional block diagram of the first-order PMD compensation system.[1]

The signal at the output of the PC board is passed through a polarizer and part of the output power is detected by photodiode PD2 through a 1% tap arm of the output power splitter. The power level detected at PD2 is used as feedback signal, and is maximized so that the signal SOP just before the polarizer is aligned with the polarizer itself. The PC is a 4-axis voltage-controlled squeezer that induces polarization rotations in a controlled way. A personal computer runs the control algorithm and manages the communication between the PD's and the PC via RS232 and USB ports, respectively.

The experiments were carried out to measure the effect of polarization scrambling on the PMD monitor signal and to find the appropriate range of

[1] The compensator was designed and built by the photonic and electromagnetic research group, Department of Information Engineering at Padova University, Italy.

scrambling frequencies for which the compensator is able to track and compensate for the SOP fluctuations.

The aim was to evaluate the capability of achieving (and maintaining) a certain DOP level within a certain time (referred to as the time step), defined as the overall number of observations divided by the total number of algorithm steps:

$$\text{Time Step} = \frac{\text{Overall observations}}{\text{Number of algorithm steps}}$$

6.1.1 Characterization of PMDC performance

A set of experiments were carried out to identify the effect of polarization scrambling on the PMD monitoring signal and to find the appropriate range of scrambling frequencies for which the compensator will be able to track and compensate for the SOP fluctuations.

The waveform generator was used to provide control signals with different periods that are applied to squeezers of a polarization controller so as to vary the SOP of the input signal. The PMDC performance was measured by its ability to achieve (and maintain) a certain SOP within a certain time frame. The choice of using the compensator time slot instead of an absolute time to measure the performance of the PMDC was motivated by the fact that the focus was to optimize the control algorithm. It is important to realise that the control algorithm is independent of the specific polarization controller hardware so that the SOP tracking speed can be readily improved by adopting faster electronic and polarization controls.

Fig. 6.2 shows the power fluctuations for the uncompensated (blue trace) and compensated signals (red trace).

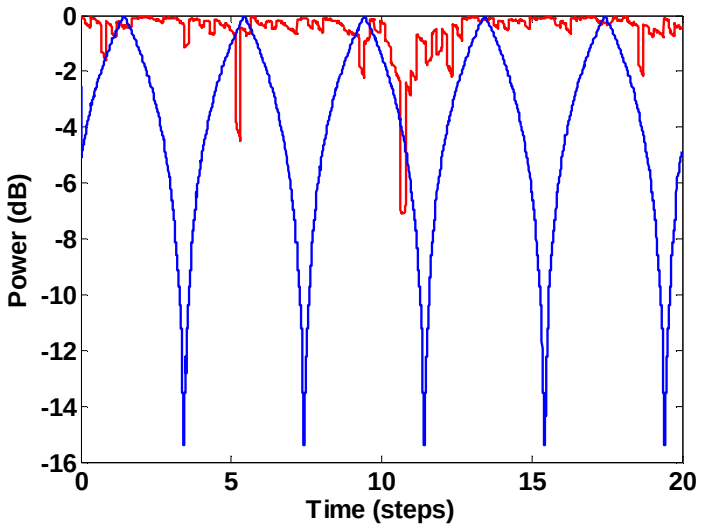

Fig. 6.2: Power fluctuations of the uncompensated (blue line) and of the compensated signals (red line) using a ramp wave signal.

When the ramp waveform generator output signal feeds the polarization scrambler, it can be seen that the power variation in the absence of compensation may be as large as 15 dB. The compensator was able to compensate for the scrambled signals with periods down to few tens of time slots. By defining the “scrambling rate” as the rate of the maximum variation of the uncompensated signal power over half a period of the scrambled signal, it can be observed that the compensator can effectively work up to 2.7 dB/step.

In a second test, the input polarization scrambler was driven with a square wave signal; in this case PMDC recovery time was analyzed, defined as the time that elapses from the abrupt variation of the input SOP to when the PMDC has reduced the insertion loss to less than 0.5 dB. The compensated and uncompensated signals together with the distribution of the recovery times are shown in Fig. 6.3.

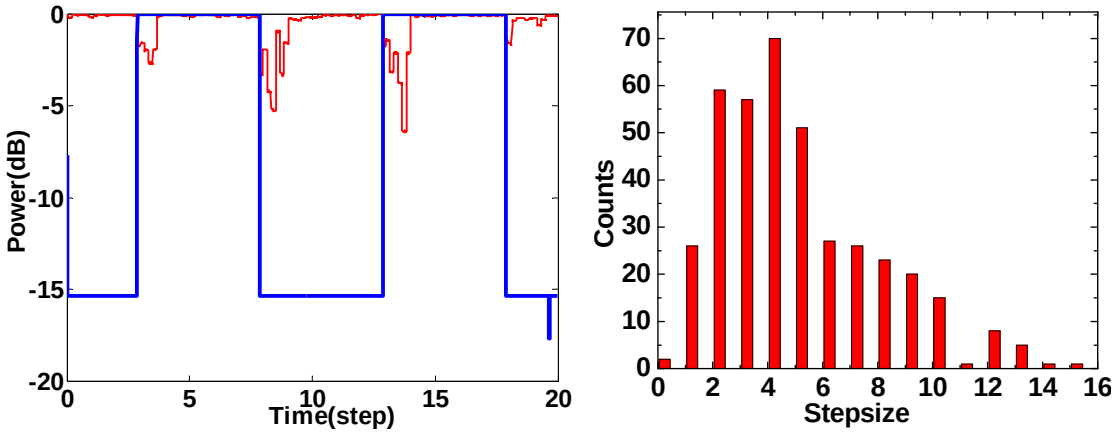

Fig. 6.3: (a) Power fluctuations of the uncompensated (blue line) and of the compensated signals (red line) using square wave signal generator. (b) Distribution of events with a maximum of 0.5 dB of PMDC excess loss for a square-wave signal applied to the input PC.

From Fig. 6.3(b), it is observed that on average, within 4 steps the PMDC is able to align the SOP of the signal to the polarizer; this confirms that the developed algorithm is highly efficient.

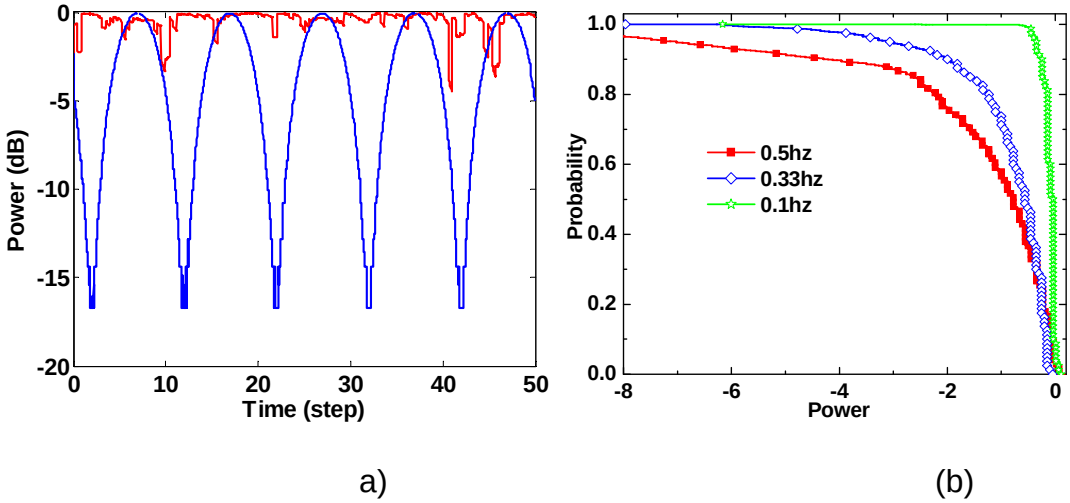

Fig. 6.4: (a) Power fluctuations of the uncompensated (blue line) and of the compensated signals (red line) using sine wave signal generator; (b) PDF vs PMDC insertion losses induced by a sine-wave variation of the input SOP for 0.45 dB/step (0.1 Hz), 0.86 dB/step (0.33 Hz) and 2.3 dB/step (0.5 Hz) respectively.

The output power of the compensated and uncompensated sine wave signal is indicated in Fig. 6.4(a), while Fig. 6.4(b) shows the Complementary Probability Cumulative Function of the PMDC insertion loss when a sinusoidal electric signal is applied to the PC. The capability of the PMDC to follow continuous SOP variations of the input signal was investigated. This situation is quite common in optical fibre links where temperature variations induce a continuous slow drift of the output SOP of the optical signal [142]. In this case, the input SOP was varied sinusoidally with different rates (defined in terms of dB/step) as it is observed in Fig. 6.4(b). It is evident from Fig 6.4(b) that if an upper limit of 1 dB for the PMDC induced insertion loss is considered, there is a probability of 100% to achieve the target for SOP variations of 0.45 dB/step and about 50% for SOP variations of 2.3 dB/step.

6.2 Evaluation of monitoring signal for multichannel PMDC

The technique used to monitor the link signal is based on monitoring the sideband DOP of the optical spectrum. When a given optical spectrum of the signal is launched into the fibre link, the DGD of the link causes the SOP of frequency components within the optical spectrum to rotate with respect to the central frequency. Since the sideband channels are more depolarized than the central channel, monitoring the sideband signals stands a high chance of compensating for all the channels in the optical spectrum. In this section the parameters that can be used to increase the sensitivity of the sideband DOP on link DGD is investigated. The monitor measures the DOP of the sideband channels and provides a single monitoring single.

The monitoring signal was determined using the factor F according to the equation below as defined in Ref [143].

$$F = 4 - (DOP_{max,\ upper} + DOP_{max,\ lower} + DOP_{min,\ upper} + DOP_{min,\ upper}) \qquad (6.1)$$

where the DOP_{min} and DOP_{max} is the minimum and maximum DOP of upper/lower sideband respectively.

However, because not only the SOP in a channel fluctuates due to DGD but also the relative inter-channel SOP rotates as a function of the channel spacing, the DOP therefore becomes insensitive to the DGD in the WDM system, causing the monitoring functionality to become inefficient. This technique has extensively been investigated by Nezam *et al* [144] by applying the modulated signals.

It is necessary therefore to find out the right channel spacing that could enhance the sideband DOP sensitivity on DGD in the link and thus increase the maximum DGD monitoring range.

Fig. 6.5 shows the experimental setup used to investigate the sensitivity of subcarrier DOP on DGD of the link. Three continuous wave (cw) signals were multiplexed and by use of the polarization controller (PC) each signal SOP was scrambled and then launched into the variable delayline, which emulated the link with changing DGD. By use of the filter at the end of the delayline, the

maximum and minimum DOPs of the output LSB and output USB signals were measured.

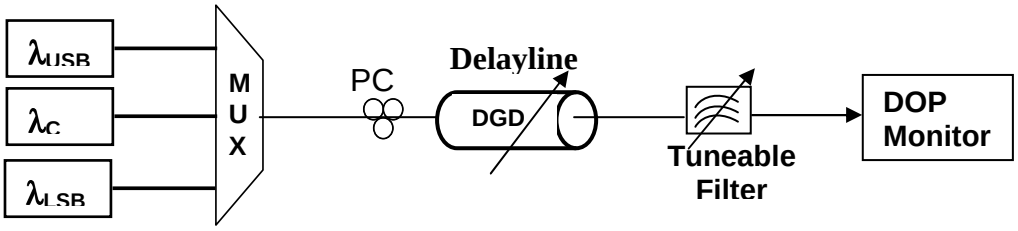

Fig. 6.5: The experimental setup to evaluate the effects of monitoring DGD on the PMD monitoring technique based on subcarrier DOP.

From these parameters F was determined as a function of the DGD of the delayline. In order to investigate the sensitivity of DOP on DGD, two experiments were carried out: first, the channel spacing of the input signals was varied as the input power was kept constant at 3 dBm, 13 dBm and 3 dBm for LSB, centre signal and USB respectively. The 50 GHz and 100 GHz channel spacings were used. Secondly, the channel spacing was kept constant at 50 GHz while the input power of the signals was varied.

The maximum DGD range is higher for 50 GHz channel spacing (30 ps) than for 100 GHz (15 ps) as observed from Fig. 6.6. This was because the numerous spectral components in such a wide bandwidth (100 GHz) could not be extinguished completely by DGD [145]. Secondly, given that the line width of the signals was narrow (<10 MHz), at that wide bandwidth the nonlinear polarization rotation effect is weak and therefore the signals require high DGD values to be depolarized. The maximum DGD range is determined at the point where the signal reaches complete depolarization. In this case the maximum depolarization occurs at the maximum value of F.

Fig. 6.6 shows the monitor signal, F, as function of DGD measured at 50 GHz (red) and 100 GHz (blue) monitoring bandwidths. In this measurement, we set the input power for LSB, centre and USB to be 3 dBm, 13 dBm and 3 dBm respectively. When the channel spacing was 50 GHz, we could obtain the monitor signal maximum sensitivity at DGD = 30 ps. However, when we increased the channel spacing to 100 GHz, the minimum value of the monitor signal was measured to be 2.75 at DGD = 17 ps.

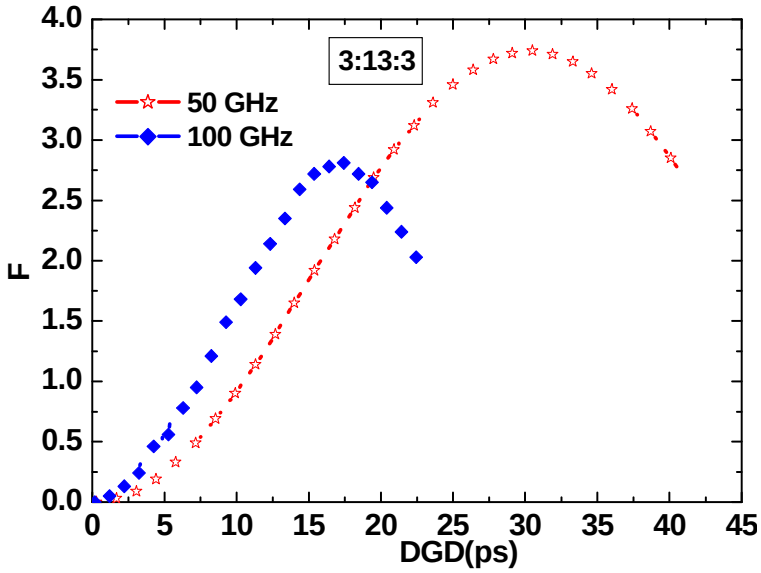

Fig. 6.6: The factor F as the function of DGD at 50 GHz and 100 GHz channel spacing measured at 13 dBm centre signal and 3 dBm for each sideband channel.

When the channel spacing was fixed at 50 GHz and the power of the centre signal was varied from 3 dBm to 13 dBm, the maximum DGD range remained constant at 30 ps for all input powers, but the signal DOP reduced with increasing power as observed in fig. 6.7. This could be due to power dependent relative SOPs in different frequencies resulting in significant depolarization and corresponding reduction in DOP.

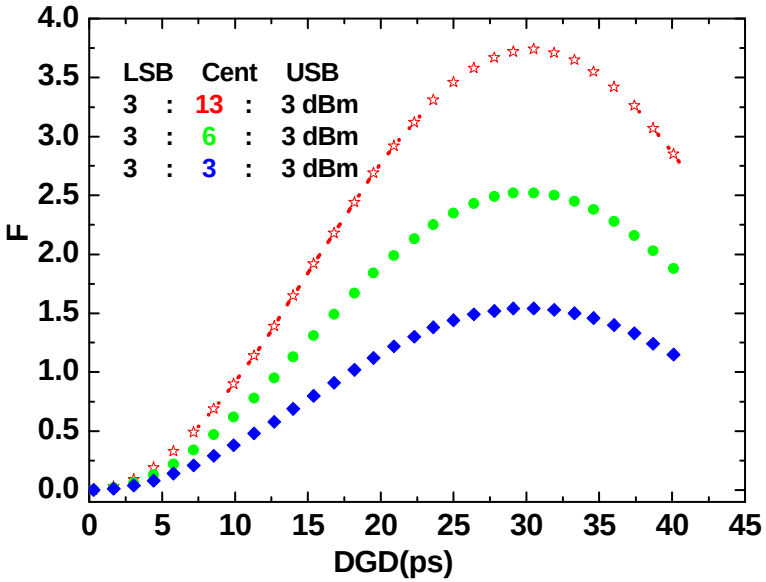

Fig. 6.7: The factor F as the function of DGD at varying centre signal input power

6.3 Operation and control of the polarization controller

The $LiNbO_3$ based polarization controller (A3200), manufactured by Adaptif Photonics Ltd was used. It has five endlessly rotatable waveplates as shown in Fig. 6.8. There are four quarter waveplates (QWP) and one half waveplate (HWP).

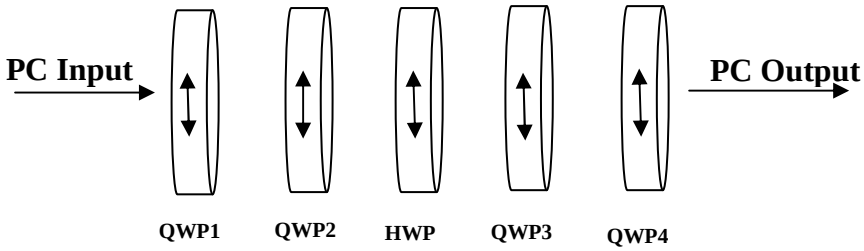

Fig. 6.8: The relative positions of the waveplates as given in the polarization controller A3200

Each plate has its own sequence of rotation. In order to achieve any arbitrary output polarization state, three waveplates are sufficient; hence only three are used for the PMD compensation application.

In order to understand how each waveplate functions an experiment was carried out where each plate was rotated through 360° and the output SOPs and DOP measured as shown in Fig. 6.9 (a). From the diagram, for QWP1 and QWP4, there is not much change in output DOP as the plates rotated through 360° while the change in angles of QWP2, HWP and QWP3 had a wide variation in DOP. Fig. 6.9 (b) shows the coverage of SOPs on the Poincaré sphere for each of the three plates, and we observe that QWP2 has the best coverage of all.

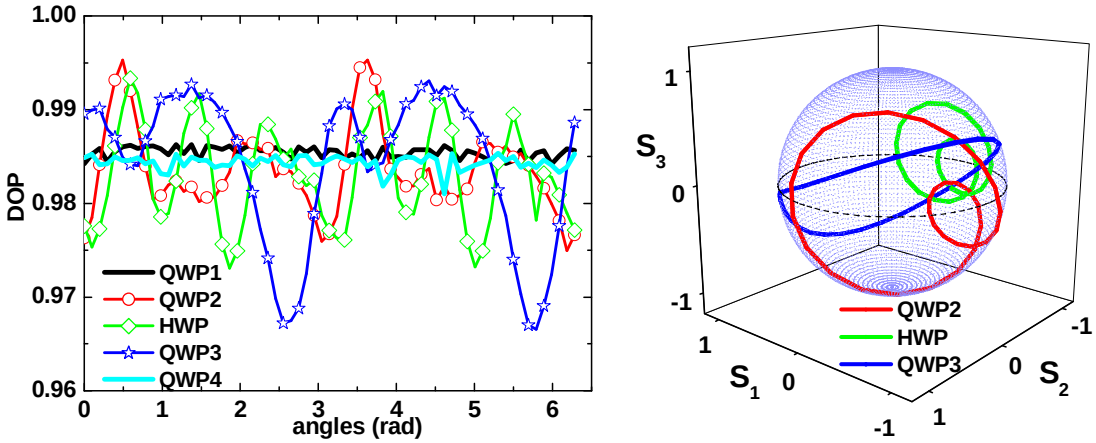

(a) (b)

Fig. 6.9: (a) minimum DOP for polarization ellipse at different waveplate angles. (b) Polarization ellipse for three waveplates each rotated through 360°.

In our compensation process we used the QWP2 alone since dithering was done just to increase the minimum DOP once the threshold point has been attained. The angles that were applied to the PC plate were generated through the General Port Interface Board (GPIB) interface board using the Labview program.

6.4 Principle of operation of the multichannel compensator

The schematic diagram shown in Fig. 6.10 was used to demonstrate the operation of the compensator. To commence the PMD compensation process, the SOPs were scrambled at the input of the link using PC1. Random polarization scrambling of the input SOP was used to improve the estimation accuracy of the output PMD vector as proposed in [92] and [146]. By tapping off a small part of the signal at the link output and filtering out the LSB and USB signals, the minimum DOP for each subcarrier was determined within one polarization scrambling period; this was used to monitor the instantaneous DGD of the link. When the minimum DOP of either LSB or USB was below the threshold value (0.95), the DGD was inferred from the lookup table and used to preset the value of the tuneable delayline.

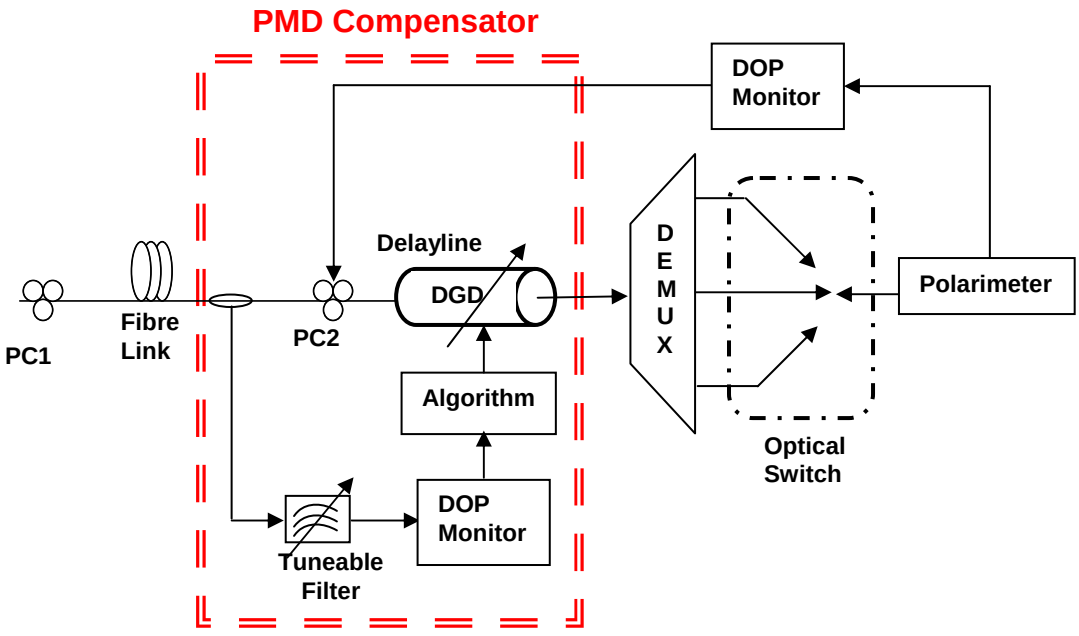

Fig.6.10: Setup for the optical PMD compensator

The output signal from the delayline was demultiplexed and by making use of the optical switch the DOP of the three channels were measured using a single polarimeter. Part of the LSB and USB output minimum DOP was tapped and used as feedback signal to the polarization controller, PC2. The settings of the PC2 were dithered to increase the minimum DOP measured. The polarization controller PC2 and variable delayline were automatically set to track this threshold operating point as it drifted in time with changing PMD.

6.5 Laboratory test

In Fig. 6.11 the three WDM sources used were operating at 1551.72 nm (Upper Sideband: λ_{USB}), 1552.12 nm (Centre wavelength: λ_C) and 1552.52 nm (Lower Sideband: λ_{LSB}) respectively. Their respective input powers were 3 dBm, 13 dBm and 3 dBm. This represented a symmetrical optical spectrum where the power falls off from the centre wavelength, and the intention was to compensate for all wavelengths within the spectrum. Polarization controller PC2 was used to align the SOPs of the centre signal parallel to the SOPs of the LSB signal which was aligned along the slow axis of the fibre input. This was done to create the worst case scenario whereby the USB signal experienced the highest depolarization possible. PC4 was used to scramble the input SOP.

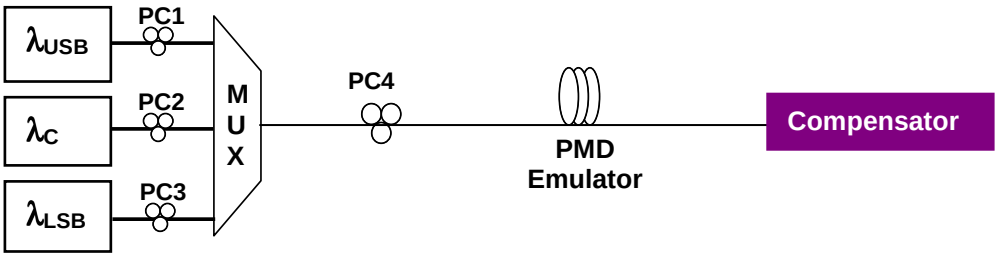

Fig. 6.11: Laboratory test compensation of PMD using the designed PMDC.

The scheme employed the PMD emulators to mimic a real fibre optic transmission system. The emulators were locally designed using a combination of polarization maintaining (PM) fibres and electro-optic polarization controllers [147]. Different emulator states were generated by randomly changing the polarization coupling inside the emulator using the distributed PCs. As is expected of ideal emulators, the DGD values from our emulators produced a Maxwellian distribution. The PMD statistics are given in Fig. 6.12 (a) and (b).

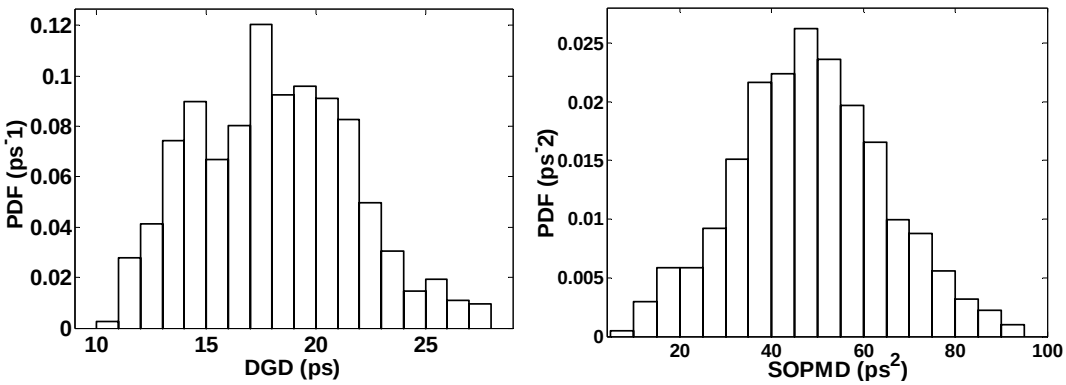

Fig. 6.12: Statistics of the PMD emulator used in our experimental work: (a) DGD statistics, (b) SOPMD statistics.

The stability of the compensator with changing input power of the sideband signals was tested. Fig. 6.13 (a) and (b) shows the results for the compensated and uncompensated DOP of the LSB and USB as a function of

time when the input power in either of the two sidebands changed from 3 dBm to 6 dBm. For the uncompensated case, when the input power of the LSB signal increased its DOP reduced, while the USB signal whose input power was kept constant had its DOP increased.

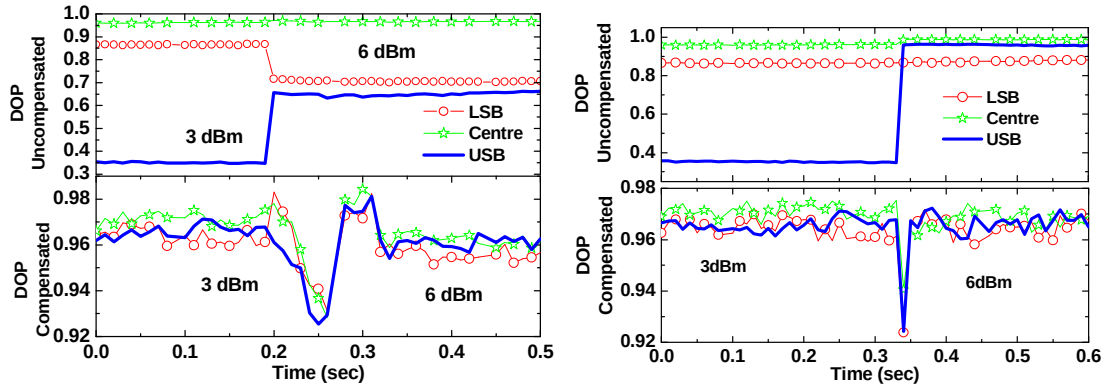

Fig. 6.13: DOP with (bottom) and without (top) compensator when input power for LSB (a) and USB (b) was changing.

On the other hand in Fig. 6.13 (b) an increase in the input power of the USB signal led to an increase in its DOP but the LSB signal was little affected. During the input power change, it is observed that the compensator was successfully able to track the SOPs in less than a second and compensate for the distorted signals. This is evident from Fig. 6.13 (b), where the compensated DOP of the three wavelengths was sustained above the threshold before and after the change of power, while before compensation the DOP for the worst channel was as low as 0.35. We therefore conclude that our compensator is able to compensate for the nonlinear PMD and is stable with change of signal power.

6.6 Field test

The experimental set up for a field test of the compensator is as shown in Fig. 6.14. The field test was carried out on a buried cable with six looped fibres installed between two Telkom exchange stations at Port Elizabeth, South Africa, with a total transmission distance of 84 km. The average first- and second-order PMD was 19 ps and 54 ps^2 respectively, measured over a wavelength range of 50 nm.

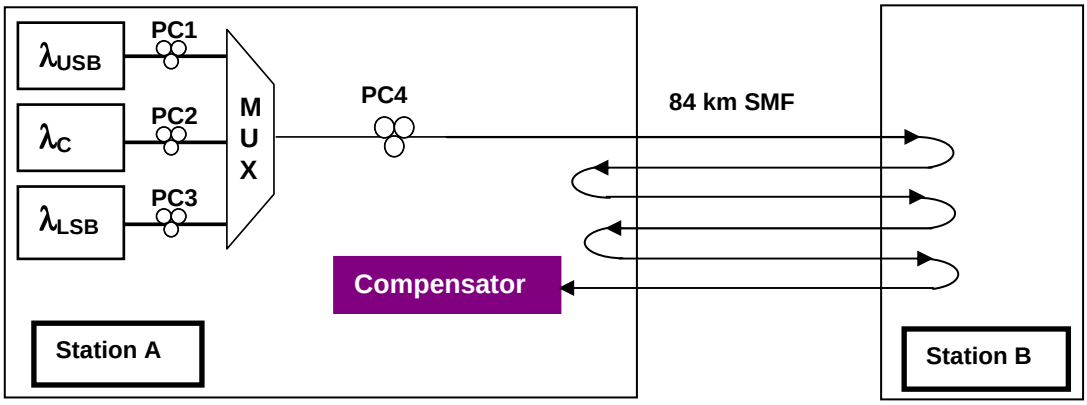

Fig. 6.14: Field test compensation of PMD using the designed PMDC.

Fig. 6.15 (a) shows the results of 23 hr continuous DOP measurement of PMDC-input and output signals for all three channels. In comparison with DOP of PMDC-input (uncompensated) signals, the DOP of the compensated signals was maintained above 0.95. This is confirmed in Fig. 6.15 (b) where the DOP distribution before and after compensation are plotted. Prior to compensation, the channel DOP was as low as 0.4 but after compensation the minimum DOP was sustained above 0.95 with an averaged DOP for compensated signals being 0.97.

It should be noted that we could not display all the data over the whole time period because of many data points. We randomly picked on the time range displayed in Fig. 6.15 (a); it has no particular significance since for the whole time period range the DOP was above 0.95.

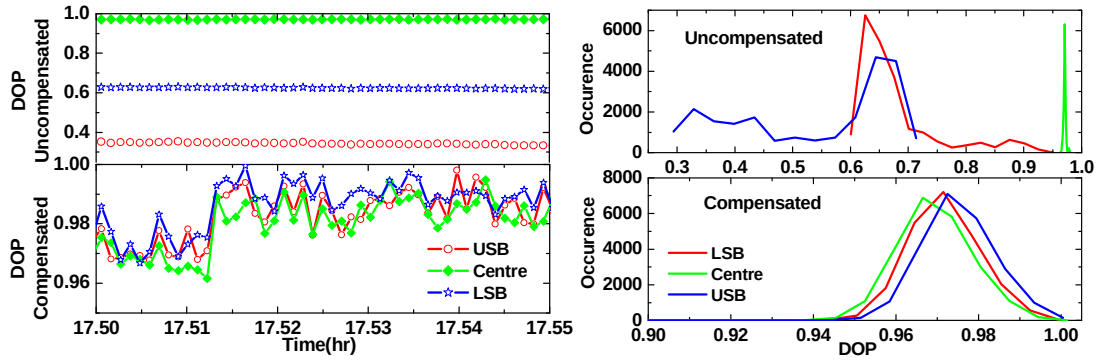

(a) (b)

Fig. 6.15: Compensating for PMD in the buried fibre at Telkom station for three channels (a) DOP for uncompensated (top) and compensated signals (bottom) (b) DOP occurrence for the uncompensated and compensated signals

6.7 Summary of results

The performance of an optical first-order PMD compensator based on a DOP-feedback technique was characterized. This was done by determining the robustness of the device in the presence of fast and wide variations of the input SOPs. All laboratory tests confirmed that our PMDC is highly efficient and reliable.

We designed an adaptive multichannel PMD compensator based on feedforward DOP-monitoring signal. It was tested at the laboratory and on a Telkom link of 84 km using buried fibre, and found to be effective. It was

shown that the monitoring signal used was sensitive to DGD up to a value of 30 ps and changing the input power of the centre signal only changed the DOP of the monitoring signal but could not increase the DGD range. Therefore the compensator is limited to compensating up to the maximum DGD of 30 ps in the link.

The results showed that our compensator introduced significant improvement in all channels within the spectrum, to the extent that the worst channels improved with more than 100 %. It has been demonstrated that both the nonlinear and the linear PMD in the communication links can be compensated effectively using the feedforward technique.

CHAPTER 7

SUMMARY AND CONCLUSIONS

The study and understanding of the interaction of PMD and nonlinearities is becoming increasingly important for long-haul optical communication networks. The interaction can be particularly complex, since the PMD in nature is stochastic and the nonlinear polarization rotation due to nonlinear induced birefringence can alter the polarization states of the bits, so that they vary from one bit to the next in a way that is difficult to predict. The effects can limit the efficiency of polarization division multiplexing and polarization interleaving based systems which use independent data sets of two orthogonal polarizations on the same frequency to double the total data throughput. In the same way, the effects make PMD compensation become impossible.

We have investigated the interaction between the PMD and nonlinear induced birefringence in a fibre with consideration of mode coupling. A sound knowledge of the interaction between PMD and nonlinear was necessary in designing a linear and nonlinear polarization mode dispersion compensator for WDM systems, which was successfully carried out.

The effect of nonlinear birefringence-induced polarization rotation in a fibre depends on the orientation of the relative input polarization vectors of co-propagated channels, and the power carried by each polarization vector. If a

polarization vector of each channel is attached to each eigenmode of the fibre, the signal is less distorted; but if the vectors are equally resolved into the two eigenmodes of the fibre, the interaction is maximized and the signals are highly depolarized. This has worked well for the networks with negligible PMD. This has been the technique that has been applied to suppress nonlinearities in WDM systems.

In section 6.2 it was revealed that in low links where the state of polarization is preserved, the nonlinear induced-birefringence effects scatter the SOPs thereby depolarizing the signal. In contrast, for signals passing through links with high polarization mode coupling, the nonlinear birefringence sometimes couples with second-order PMD such that it reduces the penalty and improves the signal DOP. It was shown that nonlinear birefringence mainly rotates the PSPs.

In the process of the investigation, polarization dependent loss (PDL) was assumed to be negligible. Since PDL causes polarization orthogonality loss, it is possible that it could impair the orthogonality between the multiplexed signals and generate coherent crosstalk on the signal in the opposite polarization state. The issue of PDL was considered to be beyond the scope of this study, and therefore we would recommend that an investigation is carried out to account for the effects of PDL in the interaction of PMD and nonlinear birefringence on the signal.

It was revealed that the nonlinear induced birefringence does not affect equally the two axes of the birefringent medium. The most affected axis has a characteristic such that there exists a critical input power of the signal above which the nonlinear birefringence suppresses linear PMD. Since the laser sources could not provide power above 13 dBm, we could not conclusively say that the less affected axis won't reach a critical point. We recommend that the investigation be carried out in this respect. Generally it is a challenge for PMD compensation in this regard where the fibre axes are differently affected.

An adaptive multichannel PMD compensator was designed with an aim of mitigating for linear and nonlinear birefringence on a channel per channel basis by monitoring the subcarrier signals. It was test at the laboratory and on the Telkom link of 84 km buried fibre loop. The compensator was found to be effective and can compensate for PMD up to maximum DGD of 30 ps. It can operate efficiently with 9 dBm power channel. The results showed that our compensator introduced a significant improvement in all channels within the spectrum, to the extent that the worst channel improved by more than 100 %.

APPENDIX I

SPECIFICATIONS OF COMPONENTS USED IN EXPERIMENTAL WORK

Components	Specification
Polarization controller/scrambler (Adaptif A3200)	SOP switching time: <10 μs Insertion loss: <3 dB PDL: <0.3 dB DGD: <0.1 ps
Polarimeter (Adaptif A1000)	Wavelength range:1460-1620 nm Sampling rate: ≤ 1 MHz
Tuneable filter	FWHM: 1.22 nm Tuneable range: 1520-1570 nm Insertion loss: 1.8 dB PDL: <0.10 dB DGD: <0.23 ps
Tuneable filter	FWHM: 0.33 nm Tuneable range: 1520-1570 nm Insertion loss: 1.8 dB PDL: <0.07 dB DGD: <0.35 ps
Variable delayline	DGD range: -65 ps to 65 ps Insertion loss: <1.5 dB
Multiplexer/Demultiplexer	No. of channels: 8 PMD: < 0.1 ps Return loss: 46 dB PDL: < 0.03 dB
Femtosecond PMD analyzer (FPMD 5600)	Wavelength range: 1530-1600 nm Measurement time: 80 s (data acquisition + calculation) PMD: < 6 fs PDL: <0.10 dB
WDM laser source (WDM8000)	Laser source: DFB laser diode Output power: <20 mW Channel spacing: ≥ 50 GHz (variable channel spacing from 50 GHz) Spectral linewidth: <10 MHz

APPENDIX II

RESEARCH OUTPUTS OF THE AUTHOR

2008

R. Cigliutti, A. Galtarossa, M. Giltrelli, D. Grosso, A. W. R. Leitch, L. Palmieri, S. Santoni, L. Schenato and D. W. Waswa, "*Design, estimation and experimental validation of optical polarization mode dispersion compensator in 40 Gbit/s NRZ AND RZ optical systems*", accepted to be published in Journal of Optical Fiber Technology.

T. B. Gibbon, L. Wu, D. W. Waswa, A. B. Conibear and A. W. R. Leitch, "*Polarization mode dispersion compensation for the South African optical-fibre telecommunication network*", S. Afr. J. Science., Vol. **104**(3), pp. 119-123 (2008).

R. Cigliutti, A. Galtarossa, M. Giltrelli, D. Grosso, A. W. R. Leitch, L. Palmieri, S. Santoni, L. Schenato and D. W. Waswa, "*Optical Polarization Mode Dispersion Compensator for 40 Gbit/s NRZ and RZ systems*", Proc. Southern African Telecommunication Networks and Applications Conference (SATNAC), Durban South Africa, paper 71, Sept 2008.

J. M. Changundega, D. W. Waswa, L. Wu and A. W. R. Leitch, "*Power Variation and Polarization State Evolution in a Two Channel WDM System*" Proc. Southern African Telecommunication Networks and Applications Conference (SATNAC), Durban, South Africa, work-in- progress paper 71, Sept 2008.

2007

D. W. Waswa, T. B. Gibbon, L. Wu and A. W. R. Leitch, **"***Impact of cross talk on polarization mode dispersion compensators"*, Proc. Southern African Telecommunication Networks and Applications Conference (SATNAC), Mauritius, paper 119, Sept 2007

2006

D. W. Waswa, T. B. Gibbon and A. W. R. Leitch, **"***Second-order PMD characterization of optical fibre using the Jones Matrix Eigenanalysis (JME) method"*, Proc. Southern African Telecommunication Networks and Applications Conference (SATNAC), Capetown, South Africa, work-in-progress paper 315, Sept 2006).

REFERENCES

[1] L. K. L. Pedrotti and S. J. Pedrotti, *"Introduction to optics",* 2nd ed., chapter **14**, Prentice Hall (1993).

[2] D. Derickson, *"Fibre optic: Test and measurement",* chapter **6**, Prentice Hall (1998).

[3] M. Born and E. Wolf, *"Principles of Optics",* 7th ed., chapter **10**, Cambridge University press (1999).

[4] S. C. Rashleigh and R. Ulrich, *"Polarization mode dispersion in single-mode fibres",* Opt. Lett., Vol. **3**(2), pp. 60-62 (1978).

[5] M. Karlsson, *"Polarization mode dispersion–induced pulse broadening in optical fibres"*, Opt. Lett., Vol. **23**(9), pp. 688-690 (1998).

[6] C. D. Poole and C. R. Giles, *"Polarization-dependent pulse compression and broadening due to polarization dispersion in dispersion-shifted fiber"*, Opt. Lett., Vol. **13**(2), pp. 155-157 (1988).

[7] J. Wuttke, P. M. Krummrich and J. Rösch, *"Polarization Oscillations in Aerial Fiber Caused by Wind and Power-Line Current"*, IEEE Photon. Technol. Lett., Vol. **15**(6), pp. 882-884 (2003).

[8] D. S. Waddy, L. Chen and X. Bao, *"Invited paper on Polarization effects in aerial fibres"*, Opt. Fiber Technol. Vol. **11**, pp.1–19 (2005).

[9] A. Galtarossa and C. R. Menyuk, *"Polarization mode dispersion"*, 1st ed., chapter **1**, Springer (2005).

[10] W. K. Burns, R. P. Moeller and C. Chen, *"Depolarization in a single-mode optical fibre"*, J. Lightwave Technol., vol. LT-1, pp. 44-50 (1983).

[11] F. Curti, B. Diano, Q. Mao and F. Matera, *"Concatenation of polarization dispersion in single-mode fibres"*, Elect. Lett., Vol. **25**(4), pp. 290-292 (1989).

[12] H. Paul, *"Polarization mode dispersion measurement by the Jones matrix Eigenanalysis and wavelength scanning methods"*, Hewlett Packard Lightwave operations Technical report, Santa Rosa, CA, USA, January 1997.

[13] A. Galtarossa and C. R. Menyuk, *"Polarization mode dispersion"*, 1st ed., chapter **2**, Springer (2005).

[14] C. D. Poole and R. W. Wagner, *"Phenomenological approach to polarization mode dispersion in long single mode fibres"*, Elect. Lett., Vol. **22**(19), pp. 1029-1030 (1986).

[15] J. P. Gordon and H. Kogelnik, *"PMD fundamentals: Polarization mode dispersion in optical fibres"*, Proceedings of National Academy of Sciences, Vol. **97**(9), pp. 4541-4550 (2000). [Online]. Available: http://www.pnas.org.

[16] C. D. Poole, N. S. Bergano, R. E. Wagner and H. J. Schulte, *"Polarization Dispersion and Principal States in a 147-km Undersea Lightwave Cable"*, J. Lightwave Technol., Vol. **6**(7), pp. 1185-1190 (1988).

[17] I. P. Kaminow and T. L. Koch, *"Optical Fibre Telecommunications: IVB Systems and impairments"*, Academic Press, San Diego, CA, Ch. **6** (1997).

[18] F. Curti, B. Daino, G. Marchis and F. Matera, *"Statistical treatment of the evolution of the principal states of polarization in single-mode fibres"*, J. Lightwave Technol., Vol. **8**(8), pp.1162-1166 (1990).

[19] W. Shieh, *"Principal states of polarization for an optical pulse"*, IEEE Photon. Technol. Lett., Vol. **11**(6), pp. 677-679 (1999).

[20] N. Gisin, R. Passy, P. Blasco, M. O. Van Deventer, R. Distl, H. Gilgen, B. Perny, R. Keys, E. Krause, C. C. Larsen, K. Mori, J. Pelayo and J. Vobian, *"Definition of polarization mode dispersion and first results of the COSTA 241 round-robin measurements"*, Pure and Appl. Opt., Vol. **4**, pp. 511-522 (1995).

[21] C. Francia, F. Bruyère, D. Penninckx and M. Chbat, *"PMD second-order effects on pulse propagation in single-mode optical fibres"*, IEEE Photon. Technol. Lett., Vol. **10**(12), pp. 1739-1741 (1998).

[22] J. N. Damask, *"Polarization Optics in Telecommunication"*, 1st Ed. Springer (2005).

[23] L. E. Nelson, R. M. Jopson, H. Kogelnik and G. J. Fischini, *"Measurement of depolarization and scaling associated with second-order polarization mode dispersion in optical fibres"*, IEEE Photon. Technol. Lett., Vol. **11**(12), pp. 1614-1616 (1999).

[24] D. Phenninckx and F. Bruyère, *"Impact of the statistics of second-order polarization mode dispersion on system performance"*, Tech. Dig. Optical Fiber Communication Conference (OFC'98), San Jose, CA, USA, pp. 340-342 (1998).

[25] F. Bruyère, *"Impact of first- and second-order PMD in optical digital transmission systems"*, Opt. Fiber Technol., Vol. **2**(3), pp. 269-280 (1996).

[26] P. Ciprut, B. Gisin, N. Gisin, R. Passy, J. P. Von der Weid, F. Prieto and C. W. Zimmer, *"Second-order polarization mode dispersion: Impact on analog and digital transmissions"*, J. Lightwave. Technol., Vol. **16**(5), pp. 757-771 (1998).

[27] E. Forestieri and G. Prati, *"Exact analytical evaluation of second-order PMD impact on the outage probability for a compensated system"*, J. Lightwave Technol., Vol. **22**(4), pp. 988-996 (2004).

[28] K. Mochizuki, Y. Namihira and H. Wakabayashi, *"Polarization mode dispersion measurements in long single mode fibres"*, Elect. Lett., 17, pp. 153-154 (1981).

[29] B. L. Heffner, *"Accurate, Automated Measurement of Differential Group Delay dispersion and Principal State Variation Using Jones Matrix Eigenanalysis"*, IEEE Photon. Technol. Lett., Vol., **5**(7), pp. 814-817 (1993).

[30] A. Galtarossa, D. Grosso, L. Palmieri and L. Schenato, *"Reflectometric characterization of hinges in optical fiber links"*, IEEE Photon. Technol. Lett., Vol. **20**(10), pp. 854- 856 (2008).

[31] F. Corsi, A. Galtarossa and L. Palmieri, *"Beat Length Characterization Based on Backscattering Analysis in Randomly Perturbed Single-Mode Fibres"*, J. Lightwave Technol. Vol. **17**(7), pp. 1172-1178 (1999).

[32] M. Wuilpart, C. Crunelle and P. Mégret, *"High dynamic polarization-OTDR for the PMD mapping in optical fiber links"*, Opt. Commun., Vol. **269**, pp. 315–321 (2007).

[33] N. Cyr, A. Girard and G. W. Schim, *"Stokes parameter analysis method, the consolidated test method for PMD measurements"*, National Fiber Optic Engineers Conference (NFOEC), EXFO electro-optic eng (1999).

[34] User Guide for Femtosecond PMD analyzer: FPMD-5600 (2002).

[35] J. Patscher and R. Eckhardt, *"Component for second-order compensation"*, Elect. Lett., Vol. **33**(3), pp. 1157-1159 (1997).

[36] L. E. Nelson, R. M. Jopson, H. Kogelnik and G. J. Foschini, *" Measurement of Depolarization and scaling associated with Second-Order Polarization Mode Dispersion in Optical Fibres"*, IEEE Photon. Technol. Lett., Vol. **11**(12), pp. 1614-1616 (1999).

[37] G. J. Foschini, R. M. Jopson, L. E. Nelson and H. Kogelnik, *"Statistics of polarization dependent chromatic fibre dispersion due to PMD"*, Proc. of European Conference of Optical Communication (ECOC),Vol. **2**(WeA2.1), pp. 56–59 (1999).

[38] M. C. De Lignie, H. G. J. Nagel and M. O. Van Deventer, *"Large polarisation mode dispersion in fiber optic cables"*, J. Lightwave. Tech**.** Vol. 12**(8)**, pp.1325-1329 (1994).

[39] A. Galtarossa, G. Gianello, C. G. Someda and M. Schiano, *"In-field comparison among polarization-mode dispersion measurement techniques"*, J. Lightwave. Tech*.* Vol. **14**(1), pp. 42-49 (1996).

[40] A. Galtarossa, M. Schiano, C. G. Someda, B. Daino, F. Matera, R. Zaninello and F. Bergamin, *"Relationship between polarisation dispersion measurements before and after installation of optical cables"*, Elect. Lett., Vol. **27**(7), pp. 595-597 (1991).

[41] K. S. Chiang, *"Conditions for obtaining zero polarisation-mode dispersion in elliptical-core fibres"*, Elect. Lett., Vol. **21**(14), pp. 592-593 (1985).

[42] K. S Chiang, *"Linearly birefringent fibres with zero polarisation-mode dispersion"*, Elect. Lett., Vol. **21**(20), pp. 916-917 (1985).

[43] A. M. Vengsarkar, A. H. Moesle, L. G. Cohen and W. L. Mammel, *"Polarization mode dispersion in dispersion shifted fibers: An exact analysis"*, Opt. Lett., Vol. **18**(17), pp. 1412-1414 (1993).

[44] C. Francia, F. Bruyere, J. P. Thiery and D. Penninckx, *"Simple dynamic polarization mode dispersion compensator"*, Elect. Lett., Vol. **35**(5), pp. 414–415 (1999).

[45] F. Heismann, D. A. Fishman and D. L. Wilson, *"Automatic Compensation of First-Order Polarization Mode Dispersion in a 10 Gb/s Transmission System"*, Proc. European Conference on Optical Communication (ECOC), Vol. **1**, pp. 529-530 (1998).

[46] F. Roy C. Francia, F. Bruyere and D. Penninckx, *"A simple dynamic polarization mode dispersion compensator"*, in Proc. Tech. Dig. OFC/IOOC Conf., Vol. **1**(TuS4), pp. 275-278 (1999).

[47] H. Bülow, *"Electronic equalization of transmission Impairements"*, in Proc. Optical Fibre Communication Conference (OFC), Vol. TuE**4**, pp. 24-25 (2002).

[48] J. H. Winters and M. A. Santoro, *"Experimental equalization of polarization dispersion"*, IEEE Photon. Technol. Lett. Vol. **2**(8) pp. 591-593(1990).

[49] D. A. Watley, K. S. Farley, B. J. Shaw, W. S. Lee, G. Bordogna, A. P. Hadjifotiou and R. E. Epworth, *"Compensation of polarization-mode dispersion exceeding one bit period using single high-birefringence fibre"*, Elect. Lett., Vol. **35**(13), pp.1094-1095 (1999).

[50] J. Poirrier, A. Gnauck and J. Winters, *"Experimental nonlinear cancellation of polarization-mode dispersion"*, in Proc. Optical Fiber Communication (OFC) Conf., Vol. **3**, pp. 119–121 (2000).

[51] W. Rosenkranz and C. Xia, *"Electrical equalization for advanced optical communication systems"*, Int. J. Elect. Commun. (AEU) Vol. **61**(3), pp. 153 – 157 (2007).

[52] F. Buchali, H. Bülow and W. Kuebart, *"Adaptive decision feedback equalization for 10 Gb/s dispersion mitigation"*, in Proc. European Conference on Optical Communication (ECOC), Vol. **2**(5.2.5), pp. 101-102 (2000).

[53] O. E. Agazzi and V. Gopinathan, *"The impact of nonlinearity on electronic dispersion compensation of optical channels"*, in Proc. Optical Fiber Communication (OFC) Conf., **TuG6**,(2004).

[54] C. R. Doerr, *"Optical Compensation of System Impairments"*, in Proc. Optical Fiber Communication Conf. (OFC), **OThL1**, (2006).

[55] H. Bülow, R. Ballentin, W. Baumert, G. Maisonneuve, G. Thielecke and T. Wehren, *"Adaptive PMD mitigation at 10 Gbit/s using an electronic SiGe equaliser IC"*, in Proc. European Conference on Optical Communication (ECOC) , Nice, France, We **C3.4** (1999).

[56] M. Schmidt, M. Witte, F. Buchali, E. Lach and H. Bülow*, "Adaptive PMD compensation for 170 Gbit/s Rz transmission systems with alternating polarisation"*, in Proc. Optical Fiber Communication (OFC) Conf., JWA**38** (2005).

[57] J. Rasmussen, A. Isomura and G. Ishikawa, *"Automatic compensation of polarization-mode dispersion for 40 Gb/s transmission systems"*, J. Lightwave Technol., Vol. **20**(12), pp. 2101-2109 (2002).

[58] H. Bülow, W. Baumert, H. Schmuck, F. Mohr, T. Schulz, F. Kuppers and W. Weiershausen *"Measurement of the maximum speed of PMD fluctuation in installed field fiber"*, In Techn. Dig. Optical Fiber communication Conf. (OFC), San Diego, CA, Paper WE**4,** pp. 83-85 (1999).

[59] H. Bülow and G. Veith, *"Temporal dynamics of error-rate degradation induced by polarization mode dispersion fluctuation of a field fiber link"*, in *Proc.* European Conference on Optical Communication (ECOC), Vol. **1**, pp. 115–118 (1997).

[60] J. A. Nagel, M. W. Chbat, L. D. Garret, J. P. Soigné, N. A. Weaver, B. M. Desthieux, H. Bülow, A. R. McCormick and R. M. Derosier, *"Long-term PMD Mitigation at 10 Gb/s and Time Dynamics over High-PMD Installed Fiber"*, in Proc. European Conference on Optical Communication (ECOC), Vol. **2**(4.2.1), pp. 31-32 (2000).

[61] R. Noė, D. Sandel, M. Yoshida-Dierolf, S. Hinz, V. Mirvoda, A. Schőpflin, C. Glingener, E. Gottwald, C. Scheerer, G. Fischer, T. Weyrauch and W. Haase, *"Polarization Mode Dispersion Compensation at 10, 20, and 40 Gb/s with Various Optical Equalizers"*, J. Lightwave. Technol., Vol. **17**(9), pp 1602-1616 (1999).

[62] S. Lee, R. Khosravani, J. Peng, V. Grubsky, D. S. Starodubov, A. E. Willner and J. Feinberg, *"Adjustable Compensation of Polarization Mode Dispersion Using a High-Birefringence Nonlinearly Chirped Fiber Bragg Grating"*, IEEE Photon. Technol. Lett., Vol. **11**(10), pp. 1277-1279 (1999).

[63] R. Pajntar, M. Vidmar*,* H. Suche, A. Paoletti and A. Schiffini, *"PMD Penalty Monitor for Automatic PMD Compensation of 40-Gb/s RZ Data"*, IEEE Photon. Technol. Lett., Vol. **16**(4), pp. 1203-1205 (2004).

[64] S. M. R. M. Nezam, L. S. Yan, Y. Q. Shi, A. E. Willner and S. Yao, *"Wide-Dynamic-range DGD monitoring by partial optical signal spectrum DOP measurement"*, Proc. of Optical Fiber Communication (OFC) Conf. pp. FD8-1- FD8-3, (2002)**.**

[65] Y. W. Song, S. M. R. Motaghian, Z. Pan and A. E. Willner, *"Efficient DOP monitoring of several WDM channels for simultaneous PMD compensation"*, Opt. Comm., Vol. **255**, pp. 225-229 (2005).

[66] S. M. R. M. Nezam, J. E. McGeehan and A. E. Willner, *"Degree-of-Polarization-Based PMD Monitoring for subcarrier- Multiplexing signals via equalized carrier/sideband filtering"*, J. Lightwave. Technol., Vol. **22**(4), pp.1078-1085 (2004).

[67] F. Buchali, S. Lanne, J. P. Thiéry, W. Baumert and H. Bűlow, *"Fast eye monitor for 10 Gb/s and its application for optical PMD compensation"*, in Proc. Fiber Optics Communication (OFC), Tu**P**, pp. 5-1 – 5-3 (2000).

[68] C. Xie and L. Mőller, *"Comparison of different feedback signals for one-stage polarization mode dispersion compensators"*, IEEE Photon. Technol. Lett., Vol. **17**(3), pp. 570-572 (2005).

[69] C. Xie and H. Haunstein, *"Optimum Length of One-Stage Polarization-Mode Dispersion Compensators with a Fixed Delay Line"*, IEEE Photon. Technol. Lett., Vol. **15**(9), pp.1228-1230 (2003).

[70] H. Rosenfeldt, R. Ulrich, U. Feiste, R. Ludwig, H. G. Weber and A. Ehrhardt, *"First-order PMD-Compensation in a 10 Gb/s NRZ Field Experiment Using Polarimetric feedback Signal"*, in Proc. European Conference on Optical Communication (ECOC), Vol. **II** (WeC3.2), pp. 134-135 (1999).

[71] T. B. Gibbon, L. Wu, D. W. Waswa, A. B. Conibear and A. W. R. Leitch, *"Polarization mode dispersion compensation for the South African optical-fibre telecommunication network"*, S. Afr. J. Science., Vol. **104**(3), pp. 119-123 (2008).

[72] T. Ono, S. Yamazaki, H. Shimizu and K. Emura, *"Polarization control method for suppressing polarization mode dispersion influence in optical transmission systems"*, J. Lightwave. Technol. Lett., Vol. **12**(5), pp. 891-898 (1994).

[73] M. Sharma, H. Ibe and T. Ozeki, *"Optical circuits for equalizing group delay dispersion of optical fibers"*, J. Lightwave. Technol. Lett., Vol. **12**(10), pp. 1759-1765 (1994).

[74] L. Möller, A. Thiede, S. Chandraekhar, W. Benz, M. Langa, T. Jakobus and M. Schlechtweg, *"ISI mitigation using decision feedback loop demonstration with PMD distorted 10 Gb/s signals"*, Elect. Lett. Vol. **35**(24), pp. 2092-2093 (1999).

[75] M. Wang, T. Li and S. Jian, *"Tunable PMD compensator based on high-birefringence linearly chirped FBG with cantilever beam"*, Opt. Exp., Vol. **11**(19), pp. 2354-2363 (2003).

[76] X. Yi, C. Lu, X. yang, W. Zhong, F. Wei and Y. Wang, *"High birefringence linearly chirped grating based optical device for PMD compensation"*, Opt. Exp., Vol. **11**(20), pp. 2634-2640.

[77] H. Bülow, *"Limitation of optical first-order PMD compensation"*, In Technol. Dig. Optical Fiber communication (OFC) Conf., San Diego, CA, USA, Vol. **2**, pp. 74-76 (1999).

[78] L. Nelson, R. M. Jopson and H. Kogelnik, *"Optical Fiber Telecommunication IVB"*, I. P. Kaminow and T. L. Koch, Eds. San Diego: Academic, Ch.**15,** pp. 740-742 (2002).

[79] G. J. Foschini, L. E. Nelson, R. M. Jopson and H. Kogelnik, *"Probability Densities of Second-Order Polarization Mode Dispersion Including Polarization Dependent Chromatic Fiber Dispersion"*, IEEE Photonics Technol. Lett., Vol. **12**(3), pp. 293-295 (2000).

[80] J. Patscher and R. Eckhardt, *"Component for second-order compensation of polarization-mode dispersion"*, Elect. Lett., Vol. **33**(13), pp. 1157-1159 (1997).

[81] Q. Yu, L. S. Yan, Y. Xie, M. Hauer and A. E. Willner, *"Higher order polarization mode dispersion compensation using fixed time delay followed by a variable time delay"*, IEEE Photon. Technol. Lett. Vol. **13**(8), pp. 863-865 (2001).

[82] M. C. Parker and S. D. Walker, *"Multiple-order PMD compensation using a single actively chirped AWG"*, in Proc. European Conference on Optical Communication (ECOC), Vol. **III** (We.p.23), pp. 424-425 (2001).

[83] T. Merker, A. Schwarzbeck and P. Meissner, *"PMD compensation up to second-order by tracking the principal states of polarization using a two-section compensator"*, Opt. Comm., Vol. **198**, pp. 41-47 (2001).

[84] L.S. Yan, Q. Yu, T. Luo, A. E. Willner and X. S. Yao, *"Compensation of higher order polarization mode dispersion using phase modulation and polarization control in the transmitter"*, IEEE Photon. Technol. Lett. Vol. **14**(6), pp. 858-860 (2001).

[85] J. Poirrier, F. Buchali, H. Bülow, S. Lanne and E. Corbel, *"Higher Order PMD canceller"*, in Proc. Optical Fiber Communication (OFC) Conf., W**14**, pp.236-237 (2002).

[86] Y. Zheng, B. Yang and X. Zhang, *"Three-Stage Polarization Mode Dispersion Compensator Capable of Compensating Second-Order Polarization Mode Dispersion"*, IEEE Photon. Technol. Lett., Vol., **14**(10), pp. 1412-1414 (2002).

[87] M. C. Parker, E. Rochat and S. D. Walker, *"All-Order PMD Compensation using Filter Theory Interpretation of Poincaré Sphere Trajectories"*, Proc. Optical Fiber Communication Conf. (OFC), ThGG**56**, pp.691-693 (2002).

[88] G. Lorenzetto, A. Galtarossa, L. Palmieri, M. Santagiustina, C. G. Someda and R. Fiorone, *"Analysis of Feedback for Higher Order Polarization-Mode Dispersion Mitigation of NRZ 40- Gb/s Optical Transmission"*, J. Lightwave. Technol. Vol. **21**(2), pp. 424-431 (2003).

[89] K. Ikeda, *"PMD Compensator with Second-Order PMD Mitigation Using Mode-Coupled Fixed Delay"*, IEEE Photon. Technol. Lett., Vol., **16**(1), pp. 105-107 (2004).

[90] P. Lu, S. J. Mihailov and L. Chen, *"The effect of variable PSP angles in a PMD compensator"*, Opt. Comm., Vol. **261**, pp. 209-212 (2006).

[91] H. Rosenfeldt, R. Ulrich, E. Brinkmeyer, U. Fieste, C. Schubert, J. Berger, R. Ludwig, H. G. Weber and A. Ehrhardt, *"Feed-forward approach for automatic PMD-Compensation at 80 Gbit/s over 45 km installed single mode fiber"*, in Proc. European Conference on Optical Communication (ECOC), Amsterdam, Netherlands, Vol. **6**, pp. 68-69 (2001).

[92] P. C. Chou, J. M. Fini and H. A. Haus, *"Real-time principal state characterization for use in PMD compensators"*, IEEE Photon. Technol. Lett., Vol. **13**(6), pp. 568-570 (2001).

[93] P. C. Chou, J. M. Fini and H. A. Haus, *"Demonstration of a feed-forward PMD compensation technique"*, IEEE Photon. Technol. Lett., Vol. **14**(2), pp. 161-163 (2002).

[94] L.S. Yan, Q. Yu, T. Luo, A. B. Sahin and A. E. Willner*, "Differential group delay monitoring used as a feedforward information for polarization mode dispersion compensation"*, IEEE Photon., Technol. Lett., Vol. **14**(10), pp.1463-1465 (2002).

[95] H. Miao and C. Yang, *"Feed-Forward Polarization-Mode Dispersion Compensation with Four Fixed Differential Group Delay Elements"*, IEEE Photon. Technol. Lett., Vol. **16**(4), pp. 1056-1058 (2004).

[96] R. Khosravani, Y. Xie, L. S. Yang, Y. W. Song, A. E. Willner and C. R. Menyuk, *"Limitations to first-order PMD Compensation in WDM system due to XPM-Induced PSP changes"*, in Proc. Optical Fiber Communication Conf. (OFC), Vol. **3**, pp. WAA5-1- WAA5-3, (2001).

[97] R. Khosravani*,* S. A. Havstad*,* Y. W. Song*,* P. Ebrahimi and A. E. Willner*, "Polarization-Mode Dispersion Compensation in WDM Systems"*, Photon. Technol. Lett., Vol. **13**(12), pp. 1370-1372 (2001).

[98] C. R. Doerr, S. Chandrasekhar, P. J. Winzer, A. R. Chraplyvy, A. H. Gnauck, L. W. Stulz, R. Pafchek and E. Burrows, *"Simple multichannel optical equalizer mitigating intersymbol interference for 40-Gb/s non-return-to-zero signals"*, J. Lightwave. Technol., Vol. **22**(1), pp. 249-256 (2004).

[99] G. E. Keiser, *"Optical Fiber Communications"*, 3rd. ed., McGraw Hill, New York, Chapter 8, 1999.

[100] K. Aiki, M. Nakamura and J. Umeda, *"A frequency-multiplexing light source with monolithically integrated distributed-feedback diode lasers"*, Quant. Elect., IEEE, Vol. **13**(4), pp. 220-223 (1977).

[101] H. Kobrinski and K. W. Cheung, ***"****Wavelength-tunable optical filters: applications and technologies"*, Communications Magazine, IEEE, Vol. **27**(10), pp.53 – 63 (1989).

[102] S. S. Dixit, *"IP over WDM: Building the next-generation optical Internet"*, John Wiley and sons, Inc. (2003).

[103] J. P. Ryan, *''WDM: North American deployment trends''*, IEEE Commun. Mag., Vol. **36**(2), pp. 40 – 44 (1998).

[104] R. J. Mears, L. Reekie, I. M. Jauncey and D. N. Payne, *"Low-noise erbium-doped fiber amplifier operating at 1.54 pm"*, Elect. Lett., Vol. **23**(2), pp. 1026-1028 (1987).

[105] I. Kaminow and T. Li, *"Optical Fiber Telecommunications IVB: Systems and Impairments"*, pp. 240, Academic Press (2002).

[106] ITU-T Recommendation, *"G.694.1 Spectral grids for WDM applications: DWDM frequency grid"* (2000).

[107] M. Wu and W. I. Way, *"Fiber nonlinearity limitations in Ultra-Dense WDM systems"*, J. Lightwave. Technol., Vol. **22**(6), pp. 1483-1498 (2004).

[108] B. Goebel, M. Kuschnerov and N. Hanik, *"On the effect of polarization-mode dispersion on the channel capacity of coherent fibre-optic*

communication systems", Proc. International conference on Transparent optical networks (ICTON),, Vol. **1(**TuD1.1), pp. 155-159 (2007).

[109] P. D. Maker and R. W. Terhune, *"Study of optical effects due to an induced polarization third order in the electric field strength"*, Phy. Rev., Vol. **137**(3A), pp. A801-A817 (1965).

[110] G. P. Agrawal, *"Nonlinear Fiber Optics"*, Academic Press, 4th ed., Chapter 2, 2007.

[111] G. P. Agrawal, *"Applications of Nonlinear Fiber Optics"*, Academic Press, 2nd ed., Chapter 5, 2008.

[112] Y. R. Shen, *"Principles of Nonlinear Optics"*, Wiley-Interscience, reprint edition, chapter 3, 1984. ISBN 0471430803.

[113] G. P. Agrawal, *"Self-phase modulation and spectral broadening of optical pulses in semiconductor laser amplifiers"*, IEEE Quant. Elect., Vol. **25**(11), pp. 2297-2306 (1989).

[114] L. F. Mollenaueer, R. H. Stolen and J. P. Gordon, *"Experimental observation of picosecond pulse narrowing and solitons in optical fibers"*, Phys. Rev. Lett., Vol. **45**(13), pp. 1095-1098 (1980).

[115] A. R. Chraplyvy, *"Limitations on lightwave communications imposed by optical-fiber nonlinearities"*, IEEE J. Lightwave. Technol., Vol. **8**(10), pp. 1548-1557 (1990).

[116] F. Forghieri, R. W. Tkach and A. R. Chraplyvy, *"Fiber Nonlinearities and Their Impact on Transmission Systems"*, in I. P. Kaminov and T. L. Koch, eds., Optical Fiber Telecommunications – III, Vol. **A**, Academic New York, Chap. 8, pp. 196-264 (1997).

[117] Z. Pan, Q. Yu, A. E. Willner and Y. Arieli, *"Fast XPM-induced polarization state fluctuations in WDM systems and their mitigation"*, in Proc. Optical Fiber Conference (OFC) 2002, Anaheim, CA, 2002, Paper ThA**7**, pp. 379–381.

[118] K. 0. Hill, D. C. Johnson, B. S. Kawasaki and R. I. MacDonald, "*CW three-wave mixing in single-mode optical fibers"*, J. Appl. Phys., Vol. **49**(10), pp. 5098-5106 (1978).

[119] N. Shibata, R. P. Braun and R. G. Waarts, *"Phase-mismatch dependence of efficiency of wave generation through four-wave mixing in a single-mode optical fiber"*, IEEE J. Quant. Elect., Vol. **QE-23**(7), pp. 1205-1210 (1987).

[120] M. W. Maeda, W. B. Sessa, W. I. Way, A. Yi-Yan, L. Curtis, R. Spicer and R. I. Laming, *"The effect of four-wave mixing in fibres on optical frequency-division multiplexed systems"*, J. Lightwave. Technol., Vol. **8**(9), pp. 1402-1408 (1990).

[121] K. Inoue and H. Toba, *"Error rate degradation due to fiber four-wave mixing in a 4-channel FSK direct detection transmission''*, IEEE Photon. Technol. Lett., Vol. **3**(1), pp. 77-79 (1991).

[122] B. C. Collings and L. Boivin, *"Nonlinear polarization evolution induced by cross-phase modulation and its impact on transmission systems"*, IEEE Photon. Technol. Lett., Vol. **12**(11), pp. 1582-1584 (2000).

[123] A. Bononi, A. Vannucci, A. Orlandini, E. Corbel, S. Lanne and S. Bigo, *"Degree of polarization degradation due to cross-phase modulation and its impact on polarization-mode dispersion compensator"*, J. Lightwave. Technol., Vol. **21**(9), pp. 1903-1913 (2003).

[124] B. Daino, G. Gregori and S. Wabnitz, *"New all-optical devices based on third-order nonlinearity of birefringent fbers"*, Opt. Lett., Vol. **11**(1), pp. 42-44 (1986).

[125] C. Vinegoni, M. Wegmemuller, B. Huttner and N. Gisin, *"Measurement of nonlinear polarization rotation in a highly birefringent optical fibre using a Faraday mirror",* J. Opt. A: Pure Appl. Opt., Vol. **2**, pp. 314-318 (2000).

[126] D. wang and C. R. Menyuk, *"Polarization Evolution due to the Kerr nonlinearity and Chromatic Dispersion"*, J. Lightwave. Technol., Vol. **17**(12), pp. 2520-2529 (1999).

[127] P. K. A. Wai and C. R. Menyuk, *"polarization mode dispersion, decorrelation and diffusion in optical fibres with randomly varying birefringence"*, J. Lightwave. Technol., Vol. **14**(2), pp. 148-157 (1996).

[128] C. Shi, *"Nonlinear Interaction of Light propagation in a birefringent optical fiber with external perturbations"*, IEEE J. Quant. Elect., Vol. **30**(6), pp.1435-1440 (1994).

[129] P. K. A. Wai, W. L. Kath, C. R. Menyuk and J. W. Zhang*, "Nonlinear polarization-mode dispersion in optical fibres with randomly varying birefringence"*, OSA J. Opt. Soc. Am. B, Vol. **14**(11), pp. 2967-2979 (1997).

[130] V. Kermène, M. T. Flores-Arias, J. Ares, A. Desfarges-Berthelemot and A. Barthélémy, *"Nonlinear polarization evolution: a numerical study of the coupling between main linear normal modes"*, Opt. Comm., Vol. **247**, pp. 195-203 (2005).

[131] S. N. Thiam and F. A. Rahman, *"A model to characterize the effect of cross phase modulation on polarization in an optical fiber transmission system"*, Optik: Intern. J. Light and Elect., Vol. **118**(7), pp. 507-514 (2007).

[132] M. Karlsson and H. Sunnerud, *"Effects of nonlinearities on PMD-induced system impairments"*, IEEE J. Lightwav. Technol., Vol. **24**(11), pp. 4127-4137 (2006).

[133] M. Bourd, M. Tur, J. Khurgin and M. Boroditsky, *"Effects of non-linearities on PMD measurements"*, in Proc. European Conference on Optical Communication (ECOC), Vol. **3**(We4.P.028), pp. 526-527 (2004).

[134] R. Khosravani, Y. W. Song, Y. Xie, L. S. Yan, A. E. Willner and C. R. Menyuk, *"Bit-pattern-dependent polarization rotation in first-order PMD-compensated WDM systems"*, Opt. Comm., Vol. **257**, pp. 191-196 (2006).

[135] E. Corbel, J. P. Thiéry, S. Lanne and S. Bigo, *"Experimental statistical assessment of XPM impact on optical PMD compensator efficiency"*, Optical Fiber Communication Conf. (OFC), Vol. **2**(ThJ2), pp. 499-501 (2003).

[136] Z. Pan, Q. Yu, Y. Ariel and A. E. Willner, *"The effects of XPM-induced fast polarization state fluctuations on PMD compensated WDM systems"*, IEEE Photon. Technol. Lett., Vol. **16**, pp.1963–1965 (2004).

[137] J. H. Lee, J. K. Park, C. H. Kim and Y. C. Chung, *"Effects of nonlinear crosstalk in optical PMD compensation"*, Photon. Technol. Lett., Vol. **14**(8), pp. 1082-1084 (2002).

[138] Virtual Photonics, Inc. (VPI), http://www.virtualphotonics.com**.**

[139] N. Gisin, J. Von der Weid and J. Pellaux, *"Polarization mode dispersion of short and long single-mode fibers"*, J. Lightwave Technol., Vol. **9**(7), pp. 821-827 (1991).

[140] H. G. Winful, *"Polarization instabilities in birefringent nonlinear media: application to fiber-optic devices"*, Opt. Lett., Vol. **11**(1), pp. 33-35 (1986).

[141] R. Cigliutti, A. Galtarossa, M. Giltrelli, D. Grosso, A. W. R. Leitch, L. Palmieri, S. Santoni, L. Schenato and D. Waswa, *"Design, estimation and experimental validation of optical Polarization Mode Dispersion Compensator in 40 Gbit/s NRZ AND RZ optical systems"*, Accepted to be published in Journal of Optical Fiber Technology.

[142] J. Haro and P. R. Horche, *"Evolution of PMD with the temperature on installed fiber"*, Opt. Fiber Technol., Vol. **14**, pp. 203–213 (2008).

[143] S. M. R. M. Nezam, J. E. McGeehan and A. E. Willner, *"Cancellation of second-order PMD effects on first-order DOP-based DGD monitors and measurement of the depolarization rate"*, in Proc. IEEE Laser and Electro-Optics Society (LEOS) Conf., **TuA3**, 2003, pp. 171-172 (2003).

[144] S. M. R. M. Nezam, L. Yan, J. E. McGeehan, Y. Shi, A. E. Willner and S. Yao, *"Enhancing the dynamic range and DGD monitoring windows in DOP-based DGD monitors using symmetric and asymmetric partial optical filtering"*, J. Lightwave Technol. **22**(4), pp. 1094-1102 (2004).

[145] J. H. Lee and Y. C. Chung, *"Optimization of monitoring bandwidth for a polarization-mode dispersion monitoring technique based on rf spectrum analysis"*, J. Opt. Netw., Vol. **5**(2), pp. 97-102 (2006).

[146] P. B. Phua, J. M. Fini and H. A. Haus, *"Real-time first and second order PMD characterization using averaged state-of-polarization of filtered signal and polarization scrambling"*, J. Lightwave Technol., Vol. **21**(4), pp. 982-989 (2003).

[147] V. Musara, L. Wu and A. W. R. Leitch, *"A Fixed Differential Group Delay but Varying Second-Order Polarization Mode Dispersion Emulator"*, In Proc. IEEE Broadband Communications, Information Technology and Biomedical Applications Conf., pp. 468-472 (2008).